

QUASI RANDOM PHYSICS-INFORMED NEURAL NETWORKS

Tianchi Yu ¹

Ivan Oseledets ²

ABSTRACT

Physics-informed neural networks have shown promise in solving partial differential equations (PDEs) by integrating physical constraints into neural network training, but their performance is sensitive to the sampling of points. Based on the impressive performance of quasi Monte-Carlo methods in high dimensional problems, this paper proposes Quasi-Random Physics-Informed Neural Networks (QRPINNs), which use low-discrepancy sequences for sampling instead of random points directly from the domain. Theoretically, QRPINNs have been proven to have a better convergence rate than PINNs. Empirically, experiments demonstrate that QRPINNs significantly outperform PINNs and some representative adaptive sampling methods, especially in high-dimensional PDEs. Furthermore, combining QRPINNs with adaptive sampling can further improve the performance.

1 INTRODUCTION

Within scientific computing, solving partial differential equations (PDEs) is central to a wide range of applications, spanning across diverse fields such as fluid dynamics Jin et al. (2021), heat transfer Özişik et al. (2017); Reddy et al. (2022), and climate prediction Saha et al. (2014). Traditional numerical methods Thomas (2013); Zienkiewicz et al. (2005); Patankar (2018) have been the cornerstone for numerical PDEs in scientific computing since the inception of scientific computing. However, these methods face challenges when dealing with high-dimensional problems. In high-dimensional PDEs, the "curse of dimensionality" limits these traditional methods, leading to a drastic and catastrophic increase in computational cost and memory requirements Constantine (2015); Trefethen (2017).

In recent years, Physics-Informed Neural Networks (PINNs) Raissi et al. (2019) have emerged as a revolutionary approach for solving numerical PDEs which can overcome the curse of dimensionality Wojtowysch & Weinan (2020); Hu et al. (2024). PINNs integrate the power of deep learning with physical laws by incorporating PDE constraints, including governing equations and their conditions, into the loss function of a neural network with their integration form. To estimate the integration by discrete points the Monte-Carlo method (MC) Kalos & Whitlock (2009) is used in PINNs. However, the performance of MC is highly sensitive to the selection and distribution of sampled points.

Many adaptive sampling strategies have been proposed to improve the performance of PINNs. Wu et al. (2023) developed the residual-based adaptive distribution (RAD) method, selecting high residual points from a candidate pool to update training sets. Peng et al. (2022) introduced RANG, a residual-based adaptive node generation method for refining collocation points in high-residual regions. Nabian et al. (2021) proposed importance sampling for efficient PINN training, prioritizing collocation points with large residuals. Gao et al. (2023) proposed FI-PINNs, defining failure probability based on residuals to enrich sampling in failure regions. Wu et al. (2024) proposed RoPINN that extends PINN from sampling isolated points to their simply connected neighborhood regions. Tang et al. (2023) introduced Adversarial Adaptive Sampling (AAS), an adversarial framework unifying PINNs and optimal transport to push residual distributions toward uniformity via Wasserstein distance. Lau et al. (2024) presented ACLE, to optimize training points using neural tangent kernel (NTK) to computing the convergence degree for every point.

¹Skolkovo Institute of Science and Technology, corresponding author: tianchi.yu@skoltech.ru.

²Skolkovo Institute of Science and Technology; AIRI.

In addition to changing the random distribution to enhance the accuracy of MC, Quasi-Monte Carlo (QMC) methods Morokoff & Caflisch (1995) are proposed to improve efficiency and convergence properties by introducing a quasi-random distribution. Based on aforementioned merits, QMC has received increasing attention in many fields, including optimization Drew & Homem-de Mello (2006), finance Goncu (2009) and particle physics Kleiss & Lazopoulos (2006). Furthermore, since QMC lacks randomness and statistical rigor, Randomized Quasi-Monte Carlo methods L'Ecuyer (2016) are proposed to add random shifts or perturbations to QMC.

In this paper, we propose the Quasi-Random Physics-Informed Neural Networks (QRPINNs), which randomly sample points from low-discrepancy sequences rather than the input domain. Because of the more evenly distributed points, the QRPINNs have impressive performance in high-dimensional PDEs. Moreover, randomly sampling from deterministic points helps implement QMC successfully in machine learning tasks by improving convergence and efficiency.

Our specific contributions can be summarized as follows:

1. We reveal that in high-dimensional PDEs, using low-discrepancy sequences is better than directly sampling from the high-dimensional domain.
2. We propose the Quasi-Random Physics-Informed Neural Networks, and theoretically prove that its convergence rate is better than PINNs.
3. We have conducted comprehensive experiments to provide convinced results that demonstrate the performance of Quasi-Random Physics-Informed Neural Networks.

The paper is structured as follows: In Section 2, we briefly introduce Physics-Informed Neural Networks, Monte-Carlo methods and Quasi-Monte Carlo methods; propose Quasi-Random Physics-Informed Neural Networks; and provide the corresponding convergence theorem and its proof. In Section 3, we compare our QRPINNs with several representative and competitive sampling methods in several equations. In Section 4, we conclude the principal findings, acknowledge the study's limitations, and discuss subsequent exploration.

2 METHODS

2.1 PHYSICS-INFORMED NEURAL NETWORKS (PINNs)

We briefly review the physics-informed neural networks (PINNs) Raissi et al. (2019) in the context of inferring the solutions of PDEs. Generally, we consider time-dependent PDEs for \mathbf{u} taking the form

$$\begin{aligned}\partial_t \mathbf{u} + \mathcal{N}[\mathbf{u}] &= 0, \quad t \in [0, T], \mathbf{x} \in \Omega, \\ \mathbf{u}(0, \mathbf{x}) &= \mathbf{g}(\mathbf{x}), \quad \mathbf{x} \in \Omega, \\ \mathcal{B}[\mathbf{u}] &= 0, \quad t \in [0, T], \mathbf{x} \in \partial\Omega,\end{aligned}\tag{1}$$

where \mathcal{N} is the differential operator, Ω is the domain of grid points, and \mathcal{B} is the boundary operator.

The ambition of PINNs is to approximate the unknown solution \mathbf{u} to the PDE system Eq. (1), by optimizing a neural network \mathbf{u}^θ , where θ denotes the trainable parameters of the neural network. The constructed loss function is:

$$\mathcal{L}(\theta) = \mathcal{L}_{ic}(\theta) + \mathcal{L}_{bc}(\theta) + \mathcal{L}_r(\theta),\tag{2}$$

where

$$\begin{aligned}\mathcal{L}_r(\theta) &= \frac{1}{N_r} \sum_{i=1}^{N_r} \varepsilon_r(\theta, t_r^i, \mathbf{x}_r^i), \quad \varepsilon_r(\theta, t, \mathbf{x}) = \left| \partial_t \mathbf{u}^\theta(t, \mathbf{x}) + \mathcal{N}[\mathbf{u}^\theta](t, \mathbf{x}) \right|^2, \\ \mathcal{L}_{ic}(\theta) &= \frac{1}{N_{ic}} \sum_{i=1}^{N_{ic}} \varepsilon_{ic}(\theta, \mathbf{x}_{ic}^i), \quad \varepsilon_{ic}(\theta, \mathbf{x}) = \left| \mathbf{u}^\theta(0, \mathbf{x}) - \mathbf{g}(\mathbf{x}) \right|^2, \\ \mathcal{L}_{bc}(\theta) &= \frac{1}{N_{bc}} \sum_{i=1}^{N_{bc}} \varepsilon_{bc}(\theta, t_{bc}^i, \mathbf{x}_{bc}^i), \quad \varepsilon_{bc}(\theta, t, \mathbf{x}) = \left| \mathcal{B}[\mathbf{u}^\theta](t, \mathbf{x}) \right|^2,\end{aligned}\tag{3}$$

corresponds to the three equations in Eq. (1) individually; $\mathbf{x}_{ic}, \mathbf{x}_{bc}, \mathbf{x}_r$ are the sampled points from the initial constraint, boundary constraint, and residual constraint, respectively; N_{ic}, N_{bc}, N_r are the total number of sampled points for each constraint, correspondingly.

2.2 MONTE-CARLO METHODS

The Monte Carlo method is a numerical method that uses random sampling to obtain numerical results. It's often used to estimate quantities that are difficult or impossible to compute exactly, especially when dealing with complex systems or high-dimensional problems. Given function $f : \mathbb{R}^d \rightarrow \mathbb{R}$, where d is the dimensionality, and the randomly sampling set $\mathcal{X} = \{\mathbf{x}_i\}_{i=1}^N$, the integration of f by Monte Carlo methods is:

$$I(f) := \int_{\Omega} f(\mathbf{x}) d\mathbf{x} \approx I_{MC}(f) := \frac{1}{N} \sum_{i=1}^N f(\mathbf{x}_i), \quad (4)$$

where $\Omega \subset \mathbb{R}^d$ is a definite set and $\mathcal{X} \subset \Omega$.

Monte Carlo methods have widely applications in several fields. For example, solving high-dimensional distribution functions in gas dynamics Moss & Bird (2005), modeling uncertainty in financial markets Glasserman (2004), and simulating systems with many coupled degrees of freedom in cellular structures Graner & Glazier (1992).

In machine learning, especially in the context of PINNs, Monte Carlo methods are used to approximate the integration of the target equations, because its convergence rate is $\mathcal{O}(N^{-1/2})$ (the proof is provided in Appendix B) which is independent of the dimensionality d .

2.2.1 MONTE CARLO METHODS IN PINNS

For a PDE system Eq. (1), suppose the analytic solution is u^* (Without loss of generality, here we consider $u \in \mathcal{H}$ that $u : \mathbb{R}^d \rightarrow \mathbb{R}$, where \mathcal{H} is the Hilbert space.) and the output solution from the network is u^{θ^*} defined as follows:

$$\theta^* := \arg \min_{\theta} \mathcal{L}(\theta). \quad (5)$$

Note that, every single equation in Eq. (3) can be regarded as a Monte Carlo approximation, *i.e.*

$$\begin{aligned} \frac{1}{N_r} \sum_{i=1}^{N_r} |\partial_t u(t_r^i, \mathbf{x}_r^i) + \mathcal{N}[u](t_r^i, \mathbf{x}_r^i)|^2 &\rightarrow \int_t \int_{\Omega} |\partial_t u(t, \mathbf{x}) + \mathcal{N}[u](t, \mathbf{x})|^2 d\mathbf{x} dt, \\ \frac{1}{N_{ic}} \sum_{i=1}^{N_{ic}} |u(0, \mathbf{x}_{ic}^i) - g(\mathbf{x}_{ic}^i)|^2 &\rightarrow \int_{\Omega} |u(0, \mathbf{x}) - g(\mathbf{x})|^2 d\mathbf{x}, \\ \frac{1}{N_{bc}} \sum_{i=1}^{N_{bc}} |\mathcal{B}[u](t_{bc}^i, \mathbf{x}_{bc}^i)|^2 &\rightarrow \int_t \int_{\partial\Omega} |\mathcal{B}[u](t, \mathbf{x})|^2 d\mathbf{x} dt, \end{aligned} \quad (6)$$

with $N_r, N_{ic}, N_{bc} \rightarrow \infty$, if the integrand is Riemann-integrable functions in $[0, T] \times \Omega$ (see Kuipers & Niederreiter (2012)). Suppose that

$$\begin{aligned} \mathcal{L}_{int}(\theta) &:= \int_t \int_{\Omega} |\partial_t u^{\theta}(t, \mathbf{x}) + \mathcal{N}[u^{\theta}](t, \mathbf{x})|^2 d\mathbf{x} dt \\ &\quad + \int_{\Omega} |u^{\theta}(0, \mathbf{x}) - g(\mathbf{x})|^2 d\mathbf{x} \\ &\quad + \int_t \int_{\partial\Omega} |\mathcal{B}[u^{\theta}](t, \mathbf{x})|^2 d\mathbf{x} dt. \\ \theta_{\infty}^* &:= \arg \min_{\theta} \mathcal{L}_{int}(\theta). \end{aligned} \quad (7)$$

Then,

$$\|u^* - u^{\theta^*}\|_{L^2(\Omega)} \leq \|u^* - u^{\theta_{\infty}^*}\|_{L^2(\Omega)} + \|u^{\theta_{\infty}^*} - u^{\theta^*}\|_{L^2(\Omega)}, \quad (8)$$

where $\Omega = [0, T] \times \Omega$. However, as u^{θ^*} is dependent on the randomly sampled points. Like Monte Carlo methods, the error analysis of the above equation requires an expectation:

$$\mathbb{E} \left[\|u^* - u^{\theta^*}\|_{L^2(\Omega)} \right] \leq \|u^* - u^{\theta^*}\|_{L^2(\Omega)} + \mathbb{E} \left[\|u^{\theta^*} - u^{\theta^*}\|_{L^2(\Omega)} \right]. \quad (9)$$

The first term $\|u^* - u^{\theta^*}\|_{L^2(\Omega)}$ depends on the size of the neural network, and the smoothness of u ; the second term $\mathbb{E} [\|u^{\theta^*} - u^{\theta^*}\|_{L^2(\Omega)}]$ depends on how well the summation represents the integration, *i.e.* the error of the Monte Carlo methods. If u is smooth and the neural network can hold that $\|u^* - u^{\theta^*}\|_{L^2(\Omega)} \ll \mathbb{E} [\|u^{\theta^*} - u^{\theta^*}\|_{L^2(\Omega)}]$, then $\mathbb{E} [\|u^* - u^{\theta^*}\|_{L^2(\Omega)}] \leq \mathbb{E} [\|u^{\theta^*} - u^{\theta^*}\|_{L^2(\Omega)}]$. Combining with Theorem 1, we can claim that, under specific requirements of the neural networks, the convergence rate of PINN is the same as the order of the quadrature. Thus, the PINNs can suffer from the curse of dimensionality theoretically.

Theorem 1. *If the PDE system is well defined and the solution $u \in \mathcal{H}$ is a smooth function, then there exists a constant r , such that for $u^\theta \in B_r(u^{\theta^*})$ where $B_r(x)$ is a compact ball with radius r , $\mathbb{E} [\|u^{\theta^*} - u^{\theta^*}\|_{L^2(\Omega)}] = \mathcal{O}(\mathbb{E} [|\mathcal{L}_{int}(\theta) - \mathcal{L}(\theta)|])$.*

Theorem 1 reveals that with enough accurate approximation, the error convergence in PINNs is dominated by the error convergence of the quadrature. We provide the proof of Theorem 1 in Appendix D.

Therefore, some strategies of adaptive sampling Wu et al. (2023); Tang et al. (2023); Gao et al. (2023) are proposed to enhance the convergence rate of the MC as well as the performance of PINNs by changing either the distribution of the sampling points or decreasing the variance of the target function which is another principle element of Monte Carlo methods (see Eq. (46)).

However, a fundamental difficulty of MC stems from the requirement that the points should be independently random samples. But in practice, there is no method to generate independent random samples concretely. On the other hand, although $P_{\mathcal{D}}(x = x_i | x \in [0, 1]) = 0 \ \forall x_i \in [0, 1]$ under any possibility distribution functions $\mathcal{D}(x)$, $P_{\mathcal{D}}(|x - x_i| < \epsilon | x \in [0, 1]) > 0$ damages the confidence and accuracy of the Monte Carlo quadrature.

2.3 QUASI MONTE-CARLO METHODS

Quasi Monte Carlo (QMC) method is proposed to accelerate the convergence rate of Monte-Carlo methods in high-dimensional integrations with low-discrepancy sequences which are chosen deterministically and methodically. QMC methods have a convergence rate $\mathcal{O}(N^{-(1-\epsilon)})$ where ϵ depends on the specific sequence and in general $\epsilon \in (0, 1)$ (see Asmussen & Glynn (2007); Hung (2024)). Furthermore, Sloan & Woźniakowski (1998) showed that when dealing with functions where the behavior varies across different dimensions with distinct weights, the convergence rate of quasi-Monte Carlo sampling can be reduced to $\mathcal{O}(N^{-1/p})$ for some $p \in [1, 2]$, which corresponds to $\epsilon = (p - 1)/p \in [0, 0.5]$.

Notably, except the theoretical convergence rate, the performance of MC and QMC is significant different in practical: the experimental error of MC is always close to the claimed convergence rate Quarteroni et al. (2006) while the practical convergence rate of QMC always larger than that of MC Paskov & Traub (1995); Gurov et al. (2016); Berblinger & Schlier (1991).

2.3.1 QUASI MONTE CARLO IN PINNS

In the context of PINNs, QMC has already been investigated to replace the MC. However, although comprehensive experiments in Wu et al. (2023) show that QMC methods perform better than MC methods in PINNs, those experiments also show that the QMC is worse than those adaptive sampling methods. We question the performance of QMC methods for the following reasons:

1. high-dimensional cases QMC is proposed to accelerate high-dimensional integrations, and has been widely applied in high-dimensional problems rather than low-dimensional problems Fang (2002); L'Ecuyer (2009); Case (2025). Thus, solving low-dimensional PDEs cannot exploit the capabilities of QMC and is unfair for QMC.

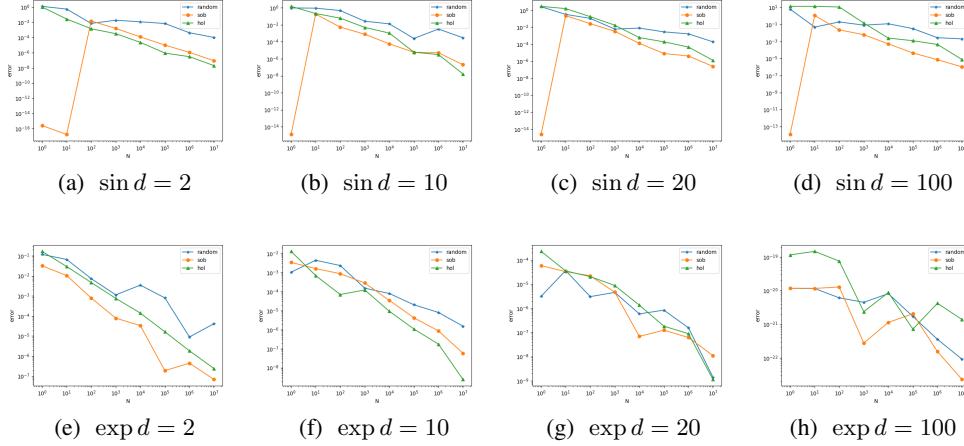


Figure 1: QMC integration for different dimensionality with different N .

We conducted a series of experiments with $f(\mathbf{x}) = \sum_{i=1}^d \sin(2\pi x_i)$, $\mathbf{x} \in [0, 1]^d$ and $f(\mathbf{x}) = \prod_{i=1}^d \exp(-x_i)$, $\mathbf{x} \in [0, 1]^d$ for different d in Fig. 1. Although some advanced papers Doerr & De Rainville (2013); Steinerberger (2019); Clément et al. (2024) provide novel approaches to generate advanced low-discrepancy sequences, the Helton sequences Halton (1960) and Sobol' sequences Sobol' (1967) are implemented in the QMC in our experiments due to the generalization and simplicity¹. The theoretically convergence rate of both Helton and Sobol' sequences is $\mathcal{O}((\log N)^d/N)$ Niederreiter (1992). But the results of Fig. 1 align the statement of aforementioned QMC researchers: although for some N and d , $\frac{(\log N)^d}{N} > \frac{1}{\sqrt{N}}$, the error of QMC is still better than MC. Furthermore, Fig. 2, which demonstrates the distribution of uniform grids, random sampling points, Halton sequences and Sobol' sequences, reveals that the points generated by random sampling are relatively scattered in an arbitrary manner, while Halton and Sobol' samplings produce point distributions that are more evenly spread out, enabling them to explore a larger portion of the domain. Obviously, this phenomenon becomes more pronounced in higher dimensions.

2. Random sampling Random sampling a batch of the total dataset is a principle strategy in machine learning to improve the performance Bottou (2010) and efficiency El Korchi & Ghanou (2019). The deterministic sequence pollutes these features and thus influences the performance. We argue that one should randomly sample points from the deterministic sequence *i.e.* regard the deterministic sequence as the total dataset and randomly sample a fixed number of points every epoch. We call it the Random Quasi Monte Carlo method (RQMC)².

However, different to MC, random sampling destroys the deterministic integration error of QMC. Herein, the error convergence of RQMC should be verified, especially when compared with MC. Notably, since every epoch will resample a batch of points, the number of untrained points is close to zero after a finite number of epochs with high possibility.

Theorem 2. For a given deterministic sequence $P_{N_{total}} = \{\mathbf{x}_i\}_{i=1}^{N_{total}}$, if $P_N = \{\tilde{\mathbf{x}}_j\}_{j=1}^N$ is a subset sampled N points from $P_{N_{total}}$. Suppose $E_{QMC} = \left| \int f(\mathbf{x})d\mathbf{x} - \frac{1}{N_{total}} \sum_{i=1}^{N_{total}} f(\mathbf{x}_i) \right| = \mathcal{O}(N_{total}^{-(1-\epsilon)})$ for some $\epsilon \in (0, 1)$ and $E_{RQMC} = \left| \int f(\mathbf{x})d\mathbf{x} - \frac{1}{N} \sum_{i=1}^N f(\tilde{\mathbf{x}}_i) \right|$, then

$$E_{RQMC} \leq \frac{dD}{2kN_{total}} + dD(1-k) + CN_{total}^{-(1-\epsilon)}, \quad (10)$$

for constant $C, D > 0, k = N/N_{total}$ and d is the dimensionality.

¹The details about Helton sequences and Sobol' sequences are provided in Appendix A

²Pay attention to the Randomized Quasi-Monte Carlo which put a random perturbation on the deterministic sequence.

Proof. Given a point set $P = \{\mathbf{x}_i\}$, the star discrepancy $D_N^*(P)$ of P is defined as follows:

Definition 1.

$$D_N^*(P) = \sup_{u_1, \dots, u_d \in [0,1]} \left| \frac{A(J; P)}{N} - \lambda_d(J) \right|, \quad (11)$$

where $J = \prod_{i=1}^d [0, u_i]$ and $\lambda_d(J) = \prod_{i=1}^d u_i$, and

$$A(J, P) = \sum_{n=1}^N \mathbb{1}_J(\mathbf{x}_n), \quad \mathbb{1}(\mathbf{x}) \text{ is the characteristic function.} \quad (12)$$

According to the error analysis of QMC³, we have.

$$E_{\text{QMC}} \leq V(f) D_{N_{\text{total}}}^*(P_{N_{\text{total}}}). \quad (13)$$

In the following proof, without loss of generality, we consider the 1D case. The following lemma is useful and its proof can be found in Kuipers & Niederreiter (2012).

Lemma 1. If $0 \leq x_1 \leq x_2 \leq \dots \leq x_N \leq 1$, then

$$D_N^*(x_1, \dots, x_N) = \frac{1}{2N} + \max_{1 \leq n \leq N} \left| x_n - \frac{2n-1}{2N} \right|. \quad (14)$$

Lemma 1 shows that the star discrepancy $D_N^*(x_1, \dots, x_N)$ is determined by the maximum absolute deviation between the points x_n and the ideal uniform grid positions $\frac{2n-1}{2N}$.

Suppose $P_{N_{\text{total}}} = \{x_i\}_{i=1}^{N_{\text{total}}}$ is the set of a given deterministic sequence in QMC that satisfies $E_{\text{QMC}} = \mathcal{O}(N_{\text{total}}^{-(1-\epsilon)})$ for a constant $\epsilon \in (0, 1)$ dependent on the given deterministic sequence, then $D_{N_{\text{total}}}^*(P_{N_{\text{total}}}) = \mathcal{O}(N_{\text{total}}^{-(1-\epsilon)})$.

Since $\frac{1}{2N} = \omega(N^{-(1-\epsilon)})$, $\forall \epsilon \in (0, 1)$, $\max_{1 \leq n \leq N_{\text{total}}} \left| x_n - \frac{2n-1}{2N_{\text{total}}} \right| \leq CN_{\text{total}}^{-(1-\epsilon)}$ i.e.

$$\left| x_n - \frac{2n-1}{2N_{\text{total}}} \right| \leq CN_{\text{total}}^{-(1-\epsilon)}, \quad \forall n \in [1, N_{\text{total}}]. \quad (15)$$

Now we consider the subset $P_N = \{\tilde{x}_j\}_{j=1}^N$. At first, we analyze the dominant term $\max_{1 \leq j \leq N} \left| \tilde{x}_j - \frac{2j-1}{2N} \right|$. Since P_N is randomly sampled from $P_{N_{\text{total}}}$, the term we actually consider is $\max_{P_N \subset P_{N_{\text{total}}}} \max_{1 \leq j \leq N} \left| \tilde{x}_j - \frac{2j-1}{2N} \right|$.

Then, we want to construct the subset $P_N^* = \arg \max_{P_N \subset P_{N_{\text{total}}}} \max_{1 \leq j \leq N} \left| \tilde{x}_j - \frac{2j-1}{2N} \right|$. Let k_j be the index of \tilde{x}_j in the original sequence ($1 \leq k_1 < k_2 < \dots < k_N \leq N_{\text{total}}$). By Eq. (15), we have $x_{k_j} \in \left[\frac{2k_j-1}{2N_{\text{total}}} - CN_{\text{total}}^{-(1-\epsilon)}, \frac{2k_j-1}{2N_{\text{total}}} + CN_{\text{total}}^{-(1-\epsilon)} \right]$. So

$$\begin{aligned} \left| \tilde{x}_j - \frac{2j-1}{2N} \right| &= \left| x_{k_j} - \frac{2j-1}{2N} \right| \\ &\leq \left| \frac{2k_j-1}{2N_{\text{total}}} - \frac{2j-1}{2N} \right| + CN_{\text{total}}^{-(1-\epsilon)} \\ &= \frac{|(2k_j-1)N - (2j-1)N_{\text{total}}|}{2NN_{\text{total}}} + CN_{\text{total}}^{-(1-\epsilon)} \end{aligned} \quad (16)$$

Thus, constructing P_N^* is equivalent to maximize the term $|(2k_j-1)N - (2j-1)N_{\text{total}}|$. Since $j \leq k_j \leq N_{\text{total}} - N + j$, the P_N^* is either the $k_j = j$ or $k_j = N_{\text{total}} - N + j$ i.e. either the first N points or the last N points. Herein, $\forall P_N \subset P_{N_{\text{total}}}$,

$$\begin{aligned} \max_{1 \leq j \leq N} \left| \tilde{x}_j - \frac{2j-1}{2N} \right| &\leq \frac{(2N-1)(N_{\text{total}}-N)}{2NN_{\text{total}}} + CN_{\text{total}}^{-(1-\epsilon)}, \\ &\leq 1 - \frac{N}{N_{\text{total}}} + CN_{\text{total}}^{-(1-\epsilon)}. \end{aligned} \quad (17)$$

³The proof is in Appendix C

Then

$$D_N^*(P_N) = \frac{1}{2N} + \max_{1 \leq j \leq N} \left| \tilde{x}_j - \frac{2j-1}{2N} \right| \leq \frac{1}{2N} + 1 - \frac{N}{N_{total}} + CN_{total}^{-(1-\epsilon)}. \quad (18)$$

Let $N = kN_{total}$, $k \in (0, 1]$,

$$D_N^*(P_N) \leq \frac{1}{2kN_{total}} + 1 - k + CN_{total}^{-(1-\epsilon)}. \quad (19)$$

Then, for d dimensional sequences,

$$D_N^*(P_N) \leq \frac{d}{2kN_{total}} + d(1 - k) + CN_{total}^{-(1-\epsilon)}. \quad (20)$$

Recall Eq. (13), we get that

$$E_{\text{RQMC}} \leq V(f)D_N^*(P_N) = \frac{dD}{2kN_{total}} + \frac{dD}{2}(1 - k) + CN_{total}^{-(1-\epsilon)}, \quad (21)$$

for $D = V(f)$. If $k = 1$, then $E_{\text{RQMC}} = \mathcal{O}(N_{total}^{-(1-\epsilon)})$.

□

Remark. Suppose N (i.e. N_{total} in Theorem 2) is the total number of the dataset, and N_b is the batch size for every epoch, and $\epsilon = N - kN$, then after s epochs, the possibility of ϵ points that have never been sampled is

$$P(\mathcal{X} = \epsilon) = \frac{\binom{N}{\epsilon} \sum_{i=0}^{N-\epsilon} (-1)^i \binom{N-\epsilon}{i} \left(\binom{(N-\epsilon)-i}{N_b} \right)^s}{\left(\binom{N}{N_b} \right)^s}. \quad (22)$$

So

$$P(\mathcal{X} = 0) = \frac{\sum_{i=0}^N (-1)^i \binom{N}{i} \left(\binom{N-i}{N_b} \right)^s}{\left(\binom{N}{N_b} \right)^s}, \quad (23)$$

which is almost 1, when $s = 20$, $N_b = 0.1N$. Thus, $k = 1$ is practical in RQMC, so the error convergence of RQMC is almost the same as the error convergence of QMC

3. Combining Under the randomly sampling idea, QMC can also combine with aforementioned adaptive sampling methods. Therefore, it is unfair to only compare the performance between QMC and adaptive sampling methods. Here we provide the algorithm of combining RAD and RQMC in Algorithm 1 as an example. Compared with the original RAD algorithm (Algorithm 3), The Algorithm 1 calculates the probability distribution on the whole low-discrepancy sequences.

Input: Dimensionality d , Number of epochs s .

Output: the output of PINN u

Generate the point pool \mathcal{P}_{pool} by d and N_{total} .

Generate \mathcal{P} by uniformly sampling from \mathcal{P}_{pool}

Train the PINN for a certain number of iterations;

for $i = 2, \dots, s$ **do**

 Generate \mathcal{P} by randomly sampling from \mathcal{P}_{pool} based on the probability distribution function:

$$p(\mathbf{x}) \propto \frac{\varepsilon_r(\theta, \mathbf{x})}{\mathbb{E}[\varepsilon_r(\theta, \mathbf{x})]} + 1, \quad (24)$$

 Train the PINN for a certain number of iterations;

end

return the output of PINN

Algorithm 1: RAD for low-discrepancy points

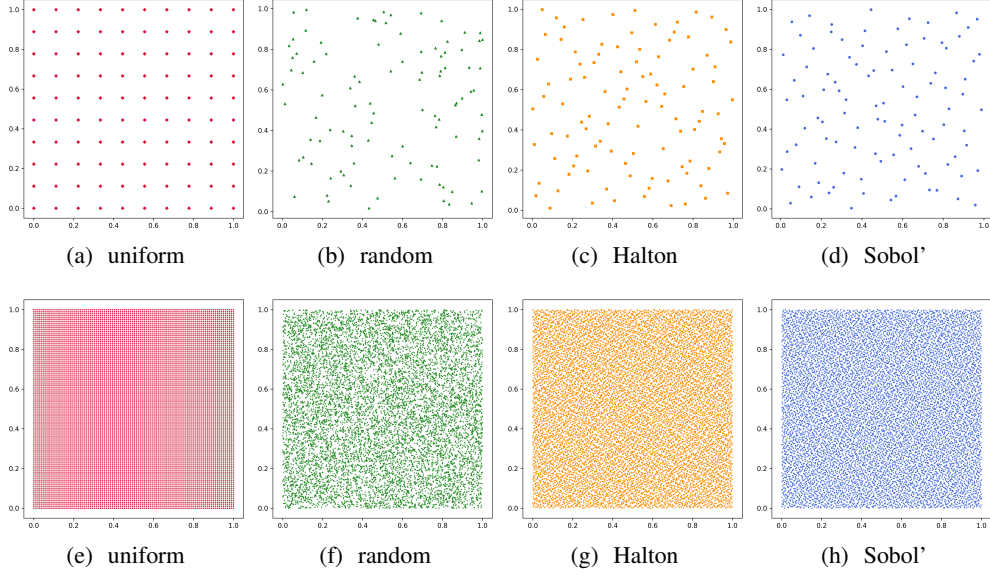


Figure 2: Examples of 100 (first row) and 10000 (second row) points generated in $[0, 1]^2$.

3 EXPERIMENTS

In the experiments, except the vanilla way (*i.e.* randomly sampling from the domain) to generate the input points, we introduce two adaptive sampling methods as baselines: 1) RAD Wu et al. (2023) is the classical adaptive sampling methods, and 2) ACLE Lau et al. (2024) is the advanced adaptive sampling methods. The details of the aforementioned methods are in Appendix E. Notably, due to the complexity of ACLE, ACLE cannot be implemented in $d = 100$ even under the estimation proposed by Lau et al. (2024).

Firstly, we consider three high-dimensional problems and conducted experiments with different dimensionality and some other hyperparameters in Section 3.1. Then we explore the cost of generating those sequences and the relationship between the accuracy in Section 3.2 and the scale of sampling pool in Section 3.3. Finally, to verify the performance of combining QRPINNs and adaptive sampling methods, we conducted experiments on ablation study in Section 3.4; to explore the limits of the dimensionality that can be effectively solved, we introduce a high-dimensional benchmark from Shi et al. (2024) in Section 3.2.

In tables, we mark out the minimum relative error by blue and we regard experiments with errors greater than 10^{-1} as failed results. The available code and hyperparameters are in GitHub at https://github.com/DUCH714/quasi_sampling_PINN.

3.1 SOLVING HIGH-DIMENSIONAL PDES

In this section, we verify three high-dimensional problems: the steady Poisson’s equations Eq. (25), the steady Allen-Cahn equations Eq. (26), and the steady Sine-Gordon equations Eq. (29)

Poisson’s equations We consider the classical high-dimensional Poisson’s equation:

$$\Delta u = f, \quad \mathbf{x} \in [-1, 1]^d, \quad (25)$$

If the solution $u(\mathbf{x}) = e^{-\alpha\|\mathbf{x}\|_2^2}$, then $f = 2\alpha(2\alpha\|\mathbf{x}\|_2^2 - d)e^{-\alpha\|\mathbf{x}\|_2^2}$. Because of the distribution of the solution has locality, Poisson equations are a classical example in adaptive sampling to verify the performance of the sampling methods.

Table 1 validates the efficiency of adaptive sampling methods in solving low-dimensional Poisson’s equations. On the contrary, when dealing with high-dimensional problems, the chosen methods become invalid, because of the complex structure in high-dimensional spaces. However, since directly

Table 1: Poisson’s equation

d	α	Vanilla	RAD	ACLE	Halton	Sobol
3	1	$3.96e-04 \pm 2.27e-04$	$2.00e-04 \pm 9.83e-05$	$9.90e-05 \pm 3.41e-05$	$6.27e-04 \pm 4.03e-04$	$2.85e-04 \pm 1.24e-04$
	10	$3.24e-03 \pm 3.39e-03$	$3.11e-03 \pm 1.84e-03$	$3.44e-03 \pm 2.67e-03$	$1.04e-03 \pm 3.30e-04$	$8.92e-04 \pm 2.25e-04$
	100	$1.28e-01 \pm 2.98e-02$	$5.51e-02 \pm 1.22e-02$	$7.68e-02 \pm 2.70e-02$	$2.35e-01 \pm 5.19e-03$	$1.48e-01 \pm 4.67e-02$
10	1	$8.09e-04 \pm 2.34e-05$	$1.04e-03 \pm 3.27e-04$	$7.98e-04 \pm 4.85e-05$	$8.38e-04 \pm 9.97e-05$	$8.23e-04 \pm 4.49e-05$
	10	$1.74e-02 \pm 4.10e-03$	$3.31e-02 \pm 1.80e-02$	$1.89e-02 \pm 2.93e-03$	$2.03e-02 \pm 6.18e-03$	$1.95e-02 \pm 4.73e-03$
	100	$1.19e+00 \pm 2.30e-01$	$1.86e+00 \pm 7.17e-01$	$1.04e+00 \pm 3.86e-02$	$1.04e+00 \pm 3.30e-02$	$5.78e+00 \pm 4.28e+00$
100	0.1	$3.15e-03 \pm 6.13e-05$	$3.19e-03 \pm 2.16e-05$	-	$3.11e-03 \pm 9.43e-06$	$3.13e-03 \pm 1.89e-05$
	1	$3.10e-02 \pm 1.70e-04$	$3.13e-02 \pm 2.49e-04$	-	$3.12e-02 \pm 8.16e-05$	$3.11e-02 \pm 1.41e-04$

randomly sampling from high-dimensional region is difficult to capture the features, combining QRPINNs with adaptive sampling methods can mitigate this challenge, resulting in better accuracy.. Those experiments are discussed in Section 3.4.

Furthermore, the adaptive sampling methods can improve the performance because it can capture the local features and make the sampling points concentrate to the locality. However, if there are enough points to capture those local features, the efficiency of adaptive sampling methods is under scrutiny. Herein, we conducted the experiments of different number of training points N_{points} . Fig. 3 demonstrates the results and indicates that the effect of adaptive sampling methods can be replaced by increasing N_{points} . Furthermore, in Fig. 3(a), the relative error of RAD and ACLE increases as N_{points} increases when N_{points} greater than a specific value and reveals that an excessive concentration of points in a specific region can lead to overfitting.

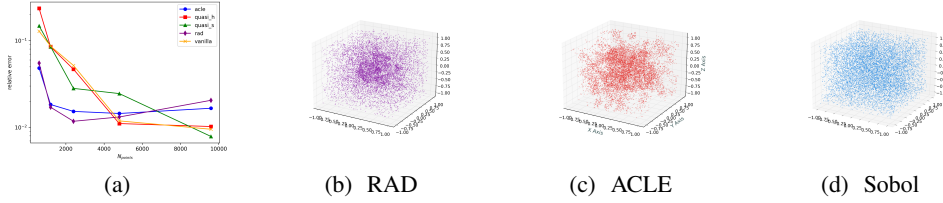


Figure 3: Poisson’s equations with $d = 3$ and $\alpha = 100$. (a) presents the relationship between the relative error and N_{points} . (b), (c), and (d) shows the distribution of training points for RAD, ACLE, and Sobol respectively.

Allen-Cahn equations We consider the steady Allen-Cahn equations:

$$\Delta u + u - u^3 = f, \mathbf{x} \in [-1, 1]^d, \quad (26)$$

we use the two-body interaction exact solution with $c_i \sim \mathcal{N}(0, 1)$:

$$u(\mathbf{x}) = \left(1 - \frac{1}{d}\|\mathbf{x}\|_2^2\right) \left(\sum_{k=1}^{d-1} c_k \sin(x_k + \cos(x_{k+1}) + x_{k+1} \sin(x_k))\right) \quad (27)$$

Let $A := \sum_{k=1}^{d-1} c_k \sin(x_k + \cos(x_{k+1}) + x_{k+1} \sin(x_k))$, $B := 1 - \frac{1}{d}\|\mathbf{x}\|_2^2$, then

$$f(\mathbf{x}) = B\Delta A + A\Delta B + \nabla A^T \nabla B + AB - A^3 B^3. \quad (28)$$

Sine-Gordon equations We consider the steady Sine-Gordon equations:

$$\Delta u + \sin(u) = f, \mathbf{x} \in [-1, 1]^d, \quad (29)$$

we use the three-body interaction exact solution with $c_i \sim \mathcal{N}(0, 1)$:

$$u(\mathbf{x}) = \left(1 - \frac{1}{d}\|\mathbf{x}\|_2^2\right) \left(\frac{1}{d-2} \sum_{i=1}^{d-2} c_i e^{x_i x_{i+1} x_{i+2}}\right) \quad (30)$$

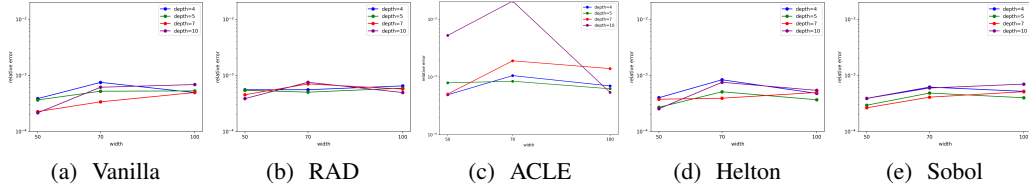


Figure 4: Allen-Cahn with $d = 3$

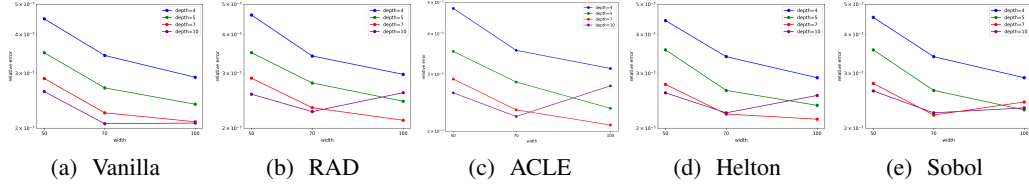


Figure 5: Allen-Cahn with $d = 10$

Let $A := \frac{1}{d-2} \sum_{i=1}^{d-2} c_i e^{x_i x_{i+1} x_{i+2}}$, $B := 1 - \frac{1}{d} \|\mathbf{x}\|_2^2$, then

$$f(\mathbf{x}) = B\Delta A + A\Delta B + \nabla A^T \nabla B + \sin(AB). \quad (31)$$

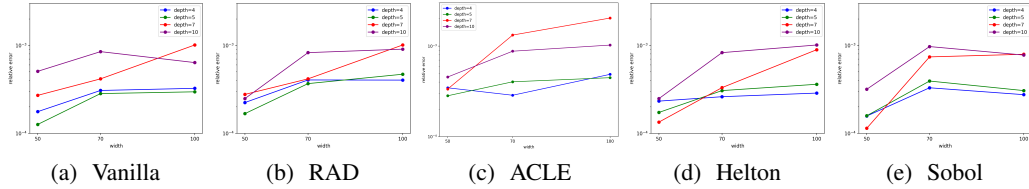


Figure 6: Sine-Gordon with $d = 3$

Results We conducted the experiments with different size of networks to verify the performance of different, the results are shown in Figs. 4 and 5 for Allen-Cahn equations with $d = 3$ and $d = 10$ respectively, Figs. 6 and 7 for Sine-Gordon equations with $d = 3$ and $d = 10$ respectively, and Fig. 8 demonstrate the results for both Allen-Cahn equations and Sine-Gordon equations with $d = 100$. The details including standard variance are provided in Appendix F.

For the Allen-Cahn equation with $d = 3$, the smallest relative error is $2.15 \times 10^{-4} \pm 3.78 \times 10^{-5}$, achieved by Vanilla with a depth of 10 and the width of 50. In the 10D case of the Allen-Cahn equation, the minimum relative error is $2.07 \times 10^{-3} \pm 3.40 \times 10^{-5}$, which is obtained by Vanilla with the depth of 10 and the width of 70. Turning to the Sine-Gordon equation in 3D, the smallest relative error is $1.14 \times 10^{-4} \pm 6.48 \times 10^{-6}$, achieved by Sobol with the depth of 7 and the width of 50. For the 10D Sine-Gordon equation, the minimum relative error is $2.09 \times 10^{-3} \pm 4.08 \times 10^{-5}$, accomplished by Vanilla when the depth is 7 and the width is 100. Although most of the best results are from the vanilla PINNs, QRPINNs outperforms these adaptive methods and reveals that adaptive methods are more suitable for low-dimensional problems and problems that have locality. On the other hand, for $d = 100$, in Fig. 8, QRPINNs achieves the best results: compared with the best results among Vanilla and RAD, QRPINNs obtain a promotion of 22.6% for Allen-Cahn equations and 32.8% for Sine-Gordon equations. Furthermore, we also conducted a series of experiments with different number of input points N_{points} , the results in Figs. 8(a) and 8(b) support that a small batch size of machine learning is necessary and can improve the performance. Hence, it is impractical to expect that increasing the number of samples in MC alone can achieve the same performance as QMC.

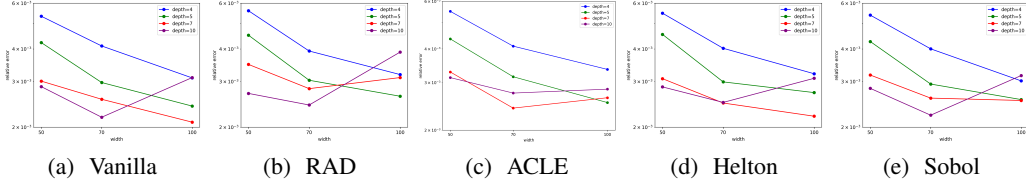


Figure 7: Sine-Gordon with $d = 10$

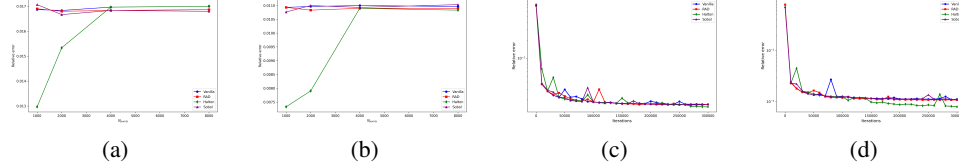


Figure 8: Sine-Gordon and Allen-Cahn with $d = 100$. (a) and (b) present the relationship between the relative error and N_{points} for Allen-Cahn and Sine-Gordon respectively. (c) and (b) illustrate the dynamic relative error during training for Allen-Cahn and Sine-Gordon respectively.

3.2 THE COST OF GENERATING LOW-DISCREPANCY SEQUENCES

In PINNs, when solving high-dimensional PDEs, it is impossible to generate a high-resolution point set by uniform grids due to the exponentially consuming of the memory. Herein, in most framework Shi et al. (2024); Cen & Zou (2024), the input points are directly generated by an uniformly random sampling on the domain Ω , *i.e.* the random sampling mentioned above. And those adaptive sampling methods will sample more points on Ω to construct the point pool and then select the input points from the point pool randomly or deterministically. However, for RQMC, the point pool is exactly the low-discrepancy sequences. Herein, if the cost of generating those sequences is also intolerable like generating the uniform grids in high-dimensionality, it is impractical to use RQMC in PINNs.

Fortunately, the cost of RQMC is acceptable, we conducted some experiments to demonstrate the relationship between cost and the number of points N as well as the dimensionality d . Fig. 9 shows that for any dimensions, the execution time is linear with the number of points and is negligible compared with the training time of PINNs. The other details including the consuming of the CPU memory can be found in Appendix G.

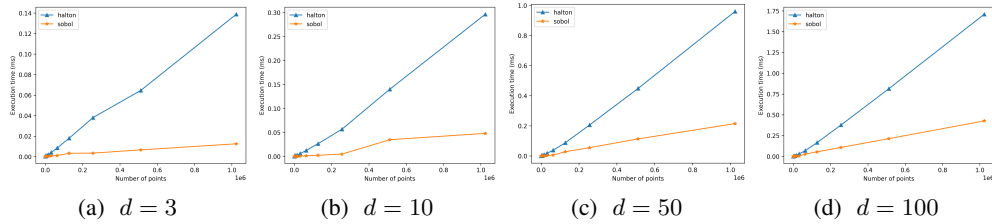


Figure 9: Execution time with different dimensionality and different number of points for Halton sequences and Sobol' sequences.

3.3 SCALE OF THE SAMPLING POOL

Although QRPINNs are training with a batch from the low-discrepancy sequence, Theorem 2 shows that with randomly sampling in a pool of low-discrepancy sequences, the scale of the pool will affect the convergence rate of the estimation. Here we conducted experiments on different N_{scale} to verify the performance and the necessity of batch size. The results, demonstrated in Fig. 10, show that with suitable N_{scale} , the performance of QRPINNs is better than $N_{scale} = 1$ *i.e.* training

with deterministic low-discrepancy sequences. Furthermore, Halton sequences are more sensitive in N_{scale} than Sobol' sequences. In the experiments of Fig. 8, we set $N_{scale} = 10$ to balance the convergence rate of PINNs and the upper bound of Theorem 2 and training 30 epochs, *i.e.* $s = 30$ in Eq. (23).

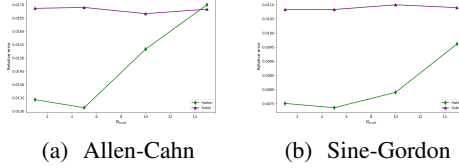


Figure 10: Relationship between relative error and N_{scale} in $d = 100$

3.4 ABLATION STUDY

As we discussed in Section 2.3.1, low-discrepancy points can be the sampling pool for those adaptive sampling methods. Herein, in this section, we demonstrate the performance for the ablation study in Poisson's equations. We choose one sampling method from $\{\text{RAD}, \text{ACLE}\}$ and one low discrepancy sequence from $\{\text{Halton}, \text{Sobol}\}$. We provide the results in Table 2 for $d = 100$. Overall, replacing the sampling pool by low-discrepancy sequences achieves better results in both $\alpha = 0.1$ and $\alpha = 1$. Furthermore, compared with Table 1, Table 2 reveals that training with the best sampling pool (Halton for $\alpha = 0.1$ and Vanilla for $\alpha = 1$) may fail to obtain the best results when combining with adaptive sampling methods. For example, when using Halton+RAD in $\alpha = 0.1$, the performance is slightly worse than that achieved by using only Halton. The discussion of $d = 3, 10$ and the ablation study of ACLE is in Appendix H.

Table 2: Ablation study $d = 100$ on Poisson's equations

α	Sampling Pool	RAD
0.1	Vanilla	$3.19e-03 \pm 2.16e-05$
	Halton	$3.14e-03 \pm 9.43e-06$
	Sobol	$3.11e-03 \pm 4.71e-06$
1	Vanilla	$3.13e-02 \pm 2.49e-04$
	Halton	$2.36e-02 \pm 2.36e-04$
	Sobol	$3.15e-02 \pm 8.16e-05$

3.5 SOLVING HIGHER DIMENSIONAL PDES BY STDE

Stochastic Taylor Derivative Estimator (STDE) Shi et al. (2024) is proposed to use stochastic Taylor derivative to estimate the derivatives in the high-dimensional space⁴. Using this estimator can solve higher dimensional PDEs more efficiently. To explore the capability of QRPINNs, we implement the Halton sequences and Sobol' sequences in STDE with $d = 10^2, 10^3, 10^4$. Here we choose the benchmark from STDE, including time-dependent semi-linear heat equation Eq. (67), time-dependent Allen-Cahn equation Eq. (68), and time-dependent Sine-Gordon equation Eq. (69). The results in Table 3 shows that except Sine-Gordon with $d = 100$ and some experiments that their relative error is in the scale of 10^{-1} , QRPINNs obtain the best error. The maximum promotion is 77.5% in Allen-Cahn with $d = 10000$ and the minimum promotion is 10.6% in Allen-Cahn with $d = 1000$. The results reveal that QRPINNs are more competitive in higher dimensionality. However, since the cost of generating low-discrepancy sequences increases with dimensionality as shown in Section 3.2, it is not practical to claim that, based on either Halton sequences or Sobol' sequences, QRPINNs are still efficient in high enough dimensionality.

⁴The details are provided in Appendix I.

Table 3: Higher dimensional PDEs					
Equation	d	Vanilla	Halton	Sobol	Promotion
Allen-Cahn	10^2	$8.12\text{e-}03 \pm 4.06\text{e-}03$	$2.54\text{e-}03 \pm 2.43\text{e-}03$	$3.01\text{e-}03 \pm 2.48\text{e-}03$	68.7%
	10^3	$1.10\text{e-}02 \pm 1.01\text{e-}02$	$2.25\text{e-}02 \pm 8.92\text{e-}03$	$9.83\text{e-}03 \pm 1.42\text{e-}02$	10.6%
	10^4	$1.55\text{e-}02 \pm 1.03\text{e-}02$	$1.49\text{e-}02 \pm 1.37\text{e-}02$	$3.48\text{e-}03 \pm 9.93\text{e-}04$	77.5%
Heat	10^2	$1.45\text{e-}02 \pm 1.20\text{e-}02$	$4.98\text{e-}02 \pm 4.62\text{e-}02$	$1.05\text{e-}02 \pm 1.02\text{e-}02$	27.6%
	10^3	$2.16\text{e-}01 \pm 7.35\text{e-}02$	$3.30\text{e-}01 \pm 1.64\text{e-}01$	$2.41\text{e-}01 \pm 9.97\text{e-}02$	-
	10^4	$2.70\text{e-}01 \pm 1.27\text{e-}01$	$3.83\text{e-}01 \pm 2.35\text{e-}01$	$3.02\text{e-}01 \pm 1.51\text{e-}01$	-
Sine-Gordon	10^2	$2.43\text{e-}02 \pm 1.05\text{e-}02$	$7.87\text{e-}02 \pm 1.73\text{e-}02$	$2.99\text{e-}02 \pm 1.90\text{e-}02$	-23.0%
	10^3	$1.03\text{e-}01 \pm 2.01\text{e-}02$	$2.04\text{e-}01 \pm 9.58\text{e-}03$	$1.62\text{e-}01 \pm 1.26\text{e-}02$	-
	10^4	$1.19\text{e-}01 \pm 4.10\text{e-}03$	$1.17\text{e-}01 \pm 8.08\text{e-}02$	$3.28\text{e-}02 \pm 3.50\text{e-}02$	72.4%

4 CONCLUSION

In this paper, we propose Quasi-Random Physics-Informed Neural Networks (QRPINNs), a novel framework that leverages low-discrepancy sequences to enhance the performance of Physics-Informed Neural Networks (PINNs), especially in solving high-dimensional PDEs. By replacing random sampling from the high-dimensional domain with random sampling from deterministic low-discrepancy sequences, QRPINNs address the inefficiency of traditional sampling in PINNs, particularly in high-dimensional PDEs.

Comprehensive experiments on high-dimensional PDEs confirm that QRPINNs outperform both traditional PINNs and competitive adaptive sampling methods. QRPINNs exhibit smaller relative errors, due to the more uniform distribution of low-discrepancy sequences, which can better capture the structure of high-dimensional spaces. The experiments indicate that although MC performs similarly to QMC under a large enough number of sampling points, the requirement of a suitable batch size ensures the necessity of RQMC in machine learning. The experiments also reveal that adaptive sampling methods become invalid when dealing with high-dimensional PDEs.

Limitations and Future work In this paper, we merely implemented two classical low-discrepancy sequences (Halton and Sobol) in QRPINNs and their computation of generating large deterministic pools will become significant in extremely high dimensions. There are more advanced sequences that can improve the convergence rate which we haven't implemented, for example modified Halton Kocis & Whiten (1997), Niederreiter Tezuka (2013) and FNN Bennett & Willemain (2004). On the other hand, some algorithms like component-by-component Baldeaux et al. (2012) and random lattice rule Goda (2025) can construct quasi-random sequences in high dimensions efficiently. Furthermore, the weighted QMC Sloan & Woźniakowski (1998); Goda (2015) may be more efficient since most high-dimensional functions merely have several principle dimensions. Finally, extending QRPINNs to couple with more adaptive strategies remains an important direction for exploration.

REFERENCES

- Søren Asmussen and Peter W Glynn. *Stochastic simulation: algorithms and analysis*, volume 57. Springer, 2007.
- Jan Baldeaux, Josef Dick, Gunther Leobacher, Dirk Nuyens, and Friedrich Pillichshammer. Efficient calculation of the worst-case error and (fast) component-by-component construction of higher order polynomial lattice rules. *Numerical Algorithms*, 59(3):403–431, 2012.
- Mihoko V Bennett and Thomas R Willemain. The filtered nearest neighbor method for generating low-discrepancy sequences. *INFORMS Journal on Computing*, 16(1):68–72, 2004.
- Michael Berblinger and Christoph Schlier. Monte carlo integration with quasi-random numbers: some experience. *Computer physics communications*, 66(2-3):157–166, 1991.

-
- Léon Bottou. Large-scale machine learning with stochastic gradient descent. In *Proceedings of COMPSTAT'2010: 19th International Conference on Computational Statistics Paris France, August 22-27, 2010 Keynote, Invited and Contributed Papers*, pp. 177–186. Springer, 2010.
- Giacomo Case. Comparative study of monte carlo and quasi-monte carlo techniques for enhanced derivative pricing. *arXiv preprint arXiv:2502.17731*, 2025.
- Jianhuan Cen and Qingsong Zou. Deep finite volume method for partial differential equations. *Journal of Computational Physics*, pp. 113307, 2024.
- François Clément, Carola Doerr, and Luís Paquete. Heuristic approaches to obtain low-discrepancy point sets via subset selection. *Journal of Complexity*, 83:101852, 2024.
- Paul G Constantine. *Active subspaces: Emerging ideas for dimension reduction in parameter studies*. SIAM, 2015.
- Carola Doerr and François-Michel De Rainville. Constructing low star discrepancy point sets with genetic algorithms. In *Proceedings of the 15th annual conference on Genetic and evolutionary computation*, pp. 789–796, 2013.
- Shane S Drew and Tito Homem-de Mello. Quas-monte carlo strategies for stochastic optimization. In *Proceedings of the 2006 winter simulation conference*, pp. 774–782. IEEE, 2006.
- Anas El Korchi and Youssef Ghanou. Unrestricted random sampling of data batch to improve the efficiency of neural networks. In *Proceedings of the New Challenges in Data Sciences: Acts of the Second Conference of the Moroccan Classification Society*, pp. 1–6, 2019.
- Kai-Tai Fang. Some applications of quasi-monte carlo methods in statistics. In *Monte Carlo and Quasi-Monte Carlo Methods 2000: Proceedings of a Conference held at Hong Kong Baptist University, Hong Kong SAR, China, November 27–December 1, 2000*, pp. 10–26. Springer, 2002.
- Zhiwei Gao, Liang Yan, and Tao Zhou. Failure-informed adaptive sampling for pinns. *SIAM Journal on Scientific Computing*, 45(4):A1971–A1994, 2023.
- Paul Glasserman. *Monte Carlo methods in financial engineering*, volume 53. Springer, 2004.
- Takashi Goda. Fast construction of higher order digital nets for numerical integration in weighted sobolev spaces. *Numerical Algorithms*, 69(2):357–396, 2015.
- Takashi Goda. A randomized lattice rule without component-by-component construction. *Mathematics of Computation*, 2025.
- Ahmet Goncu. *Monte Carlo and quasi-Monte Carlo methods in financial derivative pricing*. PhD thesis, The Florida State University, 2009.
- François Graner and James A Glazier. Simulation of biological cell sorting using a two-dimensional extended potts model. *Physical review letters*, 69(13):2013, 1992.
- Todor Gurov, Aneta Karaivanova, and Vassil Alexandrov. Energy study of monte carlo and quasi-monte carlo algorithms for solving integral equations. *Procedia Computer Science*, 80:1897–1905, 2016.
- John H Halton. On the efficiency of certain quasi-random sequences of points in evaluating multi-dimensional integrals. *Numerische Mathematik*, 2:84–90, 1960.
- Zheyuan Hu, Khemraj Shukla, George Em Karniadakis, and Kenji Kawaguchi. Tackling the curse of dimensionality with physics-informed neural networks. *Neural Networks*, 176:106369, 2024.
- Ying-Chao Hung. A review of monte carlo and quasi-monte carlo sampling techniques. *Wiley Interdisciplinary Reviews: Computational Statistics*, 16(1):e1637, 2024.
- Xiaowei Jin, Shengze Cai, Hui Li, and George Em Karniadakis. NSFnets (Navier-Stokes flow nets): Physics-informed neural networks for the incompressible Navier-Stokes equations. *Journal of Computational Physics*, 426:109951, 2021.

-
- Malvin H Kalos and Paula A Whitlock. *Monte carlo methods*. John Wiley & Sons, 2009.
- Ronald Kleiss and Achilleas Lazopoulos. Error in monte carlo, quasi-error in quasi-monte carlo. *Computer physics communications*, 175(2):93–115, 2006.
- Ladislav Kocis and William J Whiten. Computational investigations of low-discrepancy sequences. *ACM Transactions on Mathematical Software (TOMS)*, 23(2):266–294, 1997.
- Lauwerens Kuipers and Harald Niederreiter. *Uniform distribution of sequences*. Courier Corporation, 2012.
- Gregory Kang Ruey Lau, Apivich Hemachandra, See-Kiong Ng, and Bryan Kian Hsiang Low. Pinnacle: Pinn adaptive collocation and experimental points selection. *arXiv preprint arXiv:2404.07662*, 2024.
- Pierre L’Ecuyer. Quasi-monte carlo methods with applications in finance. *Finance and Stochastics*, 13:307–349, 2009.
- Pierre L’Ecuyer. Randomized quasi-monte carlo: An introduction for practitioners. In *International Conference on Monte Carlo and Quasi-Monte Carlo Methods in Scientific Computing*, pp. 29–52. Springer, 2016.
- William J Morokoff and Russel E Caflisch. Quasi-monte carlo integration. *Journal of computational physics*, 122(2):218–230, 1995.
- James N Moss and Graeme A Bird. Direct simulation monte carlo simulations of hypersonic flows with shock interactions. *AIAA journal*, 43(12):2565–2573, 2005.
- Mohammad Amin Nabian, Rini Jasmine Gladstone, and Hadi Meidani. Efficient training of physics-informed neural networks via importance sampling. *Computer-Aided Civil and Infrastructure Engineering*, 36(8):962–977, 2021.
- Harald Niederreiter. *Random number generation and quasi-Monte Carlo methods*. SIAM, 1992.
- M Necati Özişik, Helcio RB Orlande, Marcelo J Colaço, and Renato M Cotta. *Finite difference methods in heat transfer*. CRC press, 2017.
- S. H. Paskov and J. Traub. Faster evaluation of financial derivatives. *J. Portfolio Management*, 22: 113–120, 1995.
- Suhas Patankar. *Numerical heat transfer and fluid flow*. CRC press, 2018.
- Wei Peng, Weien Zhou, Xiaoya Zhang, Wen Yao, and Zheliang Liu. Rang: A residual-based adaptive node generation method for physics-informed neural networks. *arXiv preprint arXiv:2205.01051*, 2022.
- Alfio Quarteroni, Riccardo Sacco, and Fausto Saleri. *Numerical mathematics*, volume 37. Springer Science & Business Media, 2006.
- Maziar Raissi, Paris Perdikaris, and George E Karniadakis. Physics-informed neural networks: A deep learning framework for solving forward and inverse problems involving nonlinear partial differential equations. *Journal of Computational physics*, 378:686–707, 2019.
- Junuthula Narasimha Reddy, NK Anand, and Pratanu Roy. *Finite element and finite volume methods for heat transfer and fluid dynamics*. Cambridge University Press, 2022.
- Suranjana Saha, Shrinivas Moorthi, Xingren Wu, Jiande Wang, Sudhir Nadiga, Patrick Tripp, David Behringer, Yu-Tai Hou, Hui-ya Chuang, Mark Iredell, et al. The ncep climate forecast system version 2. *Journal of climate*, 27(6):2185–2208, 2014.
- Zekun Shi, Zheyuan Hu, Min Lin, and Kenji Kawaguchi. Stochastic taylor derivative estimator: Efficient amortization for arbitrary differential operators. *arXiv preprint arXiv:2412.00088*, 2024.
- Ian H Sloan and Henryk Woźniakowski. When are quasi-monte carlo algorithms efficient for high dimensional integrals? *Journal of Complexity*, 14(1):1–33, 1998.

-
- Ilya M Sobol'. The distribution of points in a cube and the approximate evaluation of integrals. *USSR Computational mathematics and mathematical physics*, 7:86–112, 1967.
- Stefan Steinerberger. A nonlocal functional promoting low-discrepancy point sets. *Journal of Complexity*, 54:101410, 2019.
- Kejun Tang, Xiaoliang Wan, and Chao Yang. DAS-PINNs: A deep adaptive sampling method for solving high-dimensional partial differential equations. *Journal of Computational Physics*, 476: 111868, 2023.
- Shu Tezuka. On the discrepancy of generalized niederreiter sequences. *Journal of Complexity*, 29 (3-4):240–247, 2013.
- James William Thomas. *Numerical partial differential equations: finite difference methods*, volume 22. Springer Science & Business Media, 2013.
- Lloyd N Trefethen. Cubature, approximation, and isotropy in the hypercube. *SIAM Review*, 59(3): 469–491, 2017.
- Pauli Virtanen, Ralf Gommers, Travis E. Oliphant, Matt Haberland, Tyler Reddy, David Cournapeau, Evgeni Burovski, Pearu Peterson, Warren Weckesser, Jonathan Bright, Stéfan J. van der Walt, Matthew Brett, Joshua Wilson, K. Jarrod Millman, Nikolay Mayorov, Andrew R. J. Nelson, Eric Jones, Robert Kern, Eric Larson, C J Carey, İlhan Polat, Yu Feng, Eric W. Moore, Jake VanderPlas, Denis Laxalde, Josef Perktold, Robert Cimrman, Ian Henriksen, E. A. Quintero, Charles R. Harris, Anne M. Archibald, Antônio H. Ribeiro, Fabian Pedregosa, Paul van Mulbregt, and SciPy 1.0 Contributors. SciPy 1.0: Fundamental Algorithms for Scientific Computing in Python. *Nature Methods*, 17:261–272, 2020.
- Sifan Wang, Xinling Yu, and Paris Perdikaris. When and why PINNs fail to train: A neural tangent kernel perspective. *Journal of Computational Physics*, 449:110768, 2022.
- Christopher Williams and Matthias Seeger. Using the nyström method to speed up kernel machines. *Advances in neural information processing systems*, 13, 2000.
- Stephan Wojtowytsch and E Weinan. Can shallow neural networks beat the curse of dimensionality? a mean field training perspective. *IEEE Transactions on Artificial Intelligence*, 1(2):121–129, 2020.
- Chenxi Wu, Min Zhu, Qinyang Tan, Yadhu Kartha, and Lu Lu. A comprehensive study of non-adaptive and residual-based adaptive sampling for physics-informed neural networks. *Computer Methods in Applied Mechanics and Engineering*, 403:115671, 2023.
- Haixu Wu, Huakun Luo, Yuezhou Ma, Jianmin Wang, and Mingsheng Long. Ropinn: Region optimized physics-informed neural networks. *arXiv preprint arXiv:2405.14369*, 2024.
- Olgiard Cecil Zienkiewicz, Robert Leroy Taylor, and Jian Z Zhu. *The finite element method: its basis and fundamentals*. Elsevier, 2005.

A SEQUENCES FOR QUASI-MONTE CARLO METHOD

A.1 HALTON SEQUENCE

Firstly, let's introduce the fractional number representation:

Definition 2. Given a base b , a fractional number $0.d_1d_2d_3\dots b$ is converted to decimal by summing each digit d_i multiplied by b^{-i} . For example, if $b = 2, d_1 = 1, d_2 = 1, d_i = 0$ for $i > 2$, then $0.11_2 = 1 \cdot 2^{-1} + 1 \cdot 2^{-2} = 0.75$.

Let p_1, p_2, \dots, p_d be the first d prime numbers, where d is the dimensionality. The Halton sequence $\mathbf{x}_0, \mathbf{x}_1, \dots$ is given by

$$\mathbf{x}_i = (\phi_{p_1}(i), \phi_{p_2}(i), \dots, \phi_{p_d}(i)), \quad i = 0, 1, \dots, \quad (32)$$

where $\phi_b(i) := \sum_{a=1}^{\infty} \frac{i_a}{b^a}$. Explicit expression is as follows,

$$\begin{aligned} \mathbf{x}_0 &= (0, 0, 0, \dots, 0) \\ \mathbf{x}_1 &= (0.1_2, 0.1_3, 0.1_5, \dots, 0.1_{p_d}) \\ \mathbf{x}_2 &= (0.01_2, 0.2_3, 0.2_5, \dots, 0.2_{p_d}) \\ \mathbf{x}_3 &= (0.11_2, 0.01_3, 0.3_5, \dots, 0.3_{p_d}) \\ &\vdots \end{aligned} \tag{33}$$

In our experiments, the prime number starts from 2.

A.2 SOBOL' SEQUENCE

Suppose the sequence is $\mathbf{x}_0, \mathbf{x}_1, \dots$, and $\mathbf{t}_i = (t_{i,1}, t_{i,2}, \dots, t_{i,d})$, Sobol' sequence is expressed by:

$$t_{i,j} = i_0 v_{1,j} \oplus i_1 v_{2,j} \oplus \dots \oplus i_{r-1} v_{r,j}, \tag{34}$$

where \oplus is the bitwise XOR operator, i_r is generated by the dyadic expansion of index i : $i = i_0 + 2i_1 + \dots + 2^{r-1}i_{r-1}$, and the direction numbers $v_{k,j}$ is defined by:

$$v_{k,j} := \frac{m_{k,j}}{2^k}, \tag{35}$$

where $m_{k,j}$ is generated as follows:

Let $p_1, \dots, p_d \in \mathbb{Z}_2[x]$ be distinct primitive polynomials ordered according to their degree, and let

$$p_j(x) = x^{e_j} + a_{1,j}x^{e_j-1} + a_{2,j}x^{e_j-2} + \dots + a_{e_j-1,j}x + 1, \quad \text{for } 1 \leq j \leq d, \tag{36}$$

where $a_{j,k} \in \mathbb{Z}_2$ is the coefficient of the polynomial p_j and e_j is the degree of p_j .

Then we can define $m_{k,j}$ for every $j \in [1, d]$, if $1 \leq k \leq e_j$, choose odd natural numbers $1 \leq m_{1,j}, \dots, m_{e_j,j}$ such that $m_{k,j} < 2^k$, and if $k > e_j$, define $m_{k,j}$ recursively by

$$m_{k,j} = 2a_{1,j}m_{k-1,j} \oplus \dots \oplus 2^{e_j-1}a_{e_j-1,j}m_{k-e_j+1,j} \oplus 2^{e_j}m_{k-e_j,j} \oplus m_{k-e_j,j}. \tag{37}$$

In conclusion,

$$m_{k,j} = \begin{cases} \text{odd nature numbers,} & \text{for } k < e_j, \\ a_{1,j}m_{k-1,j} \oplus \dots \oplus 2^{e_j-1}a_{e_j-1,j}m_{k-e_j+1,j} \oplus 2^{e_j}m_{k-e_j,j} \oplus m_{k-e_j,j}, & \text{for } k > e_j. \end{cases} \tag{38}$$

In totally, the whole algorithm for generating Sobol' sequence is provided in Algorithm 2.

Input: Dimensionality d , number of points N , primitive polynomials p_1, \dots, p_d .

Output: Sobol' sequence t_0, t_1, \dots, t_{N-1} in $[0, 1]^d$.

Compute $m_{k,j}$ by Eq. (38) and $v_{k,j}$ by Eq. (35) for $j = 1$ to d and $k = 1$ to $\lceil \log_2 N \rceil$;

for $i = 0, \dots, N-1$ **do**

 Convert i to binary: $i = \sum_{r=0}^{\infty} i_r 2^r$;

for $j = 1, \dots, d$ **do**

$t_{i,j} = \bigoplus_{r=0}^{\infty} i_r v_{r+1,j}$;

end

end

return t_0, t_1, \dots, t_{N-1} .

Algorithm 2: Sobol' sequence generation

B PROOF OF THE CONVERGENCE RATE OF MONTE CARLO METHOD

Here we give a brief proof of 1D Monte Carlo method under the uniform sampling distribution.

Proof. The Monte Carlo method approximates the quadrature of a function $f : [0, 1] \rightarrow \mathbb{R}$ by a summation of a randomly sampling set $\{x_i\}_{i=1}^N$, i.e.:

$$I(f) := \int_0^1 f(x)dx \approx I_{\text{MC}}(f) := \frac{1}{N} \sum_{i=1}^N f(x_i). \tag{39}$$

The error of the Monte Carlo integration is:

$$E_{MC} = |I(f) - I_{MC}(f)|. \quad (40)$$

However, as the set is sampled randomly, so it is impossible to obtain a deterministic error of Monte Carlo method. Hence, we consider the expectation of the square of E_{MC} :

$$\mathbb{E} [|I(f) - I_{MC}(f)|^2] = \mathbb{E} [I_{MC}(f)^2] - 2\mathbb{E} [I_{MC}(f)] I(f) + I(f)^2, \quad (41)$$

As

$$\begin{aligned} \mathbb{E} [I_{MC}(f)] &= \int_{[0,1]} \cdots \int_{[0,1]} \left(\frac{1}{N} \sum_{i=1}^N f(x_i) \right) dx_1 \dots dx_N \\ &= \frac{1}{N} \sum_{i=1}^N I(f) \\ &= I(f), \end{aligned} \quad (42)$$

and

$$\begin{aligned} \mathbb{E} [I(f)^2] &= \int_{[0,1]} \cdots \int_{[0,1]} \left(\frac{1}{N} \sum_{i=1}^N f(x_i) \right)^2 dx_1 \dots dx_N \\ &= \int_{[0,1]} \cdots \int_{[0,1]} \left(\frac{1}{N^2} \sum_{i=1}^N \sum_{k=1}^N f(x_i) f(x_k) \right) dx_1 \dots dx_N \\ &= \int_{[0,1]} \cdots \int_{[0,1]} \left(\frac{1}{N^2} \sum_{i=1}^N f^2(x_i) + \frac{1}{N^2} \sum_{i=1}^N \sum_{\substack{k=1 \\ k \neq i}}^N f(x_i) f(x_k) \right) dx_1 \dots dx_N \\ &= \frac{1}{N^2} \sum_{i=1}^N \int_{[0,1]} f^2(x_i) dx_i + \frac{1}{N^2} \sum_{i=1}^N \sum_{\substack{k=1 \\ k \neq i}}^N \int_{[0,1]} f(x_i) dx_i \int_{[0,1]} f(x_k) dx_k \\ &= \frac{1}{N} I(f^2) + \frac{N-1}{N} I(f)^2. \end{aligned} \quad (43)$$

Consequently,

$$\begin{aligned} \mathbb{E} [|I(f) - I_{MC}(f)|^2] &= \frac{1}{N} I(f^2) + \frac{N-1}{N} I(f)^2 - 2I(f)^2 + I(f)^2 \\ &= \frac{I(f^2) - I(f)^2}{N}. \end{aligned} \quad (44)$$

Hence, we obtain that

$$\begin{aligned} \mathbb{E} [I_{MC}(f)] &= I(f), \\ \text{Var} [I_{MC}(f)] &= \mathbb{E} [|I(f) - I_{MC}(f)|^2] = \frac{I(f^2) - I(f)^2}{N}. \end{aligned} \quad (45)$$

Suppose $\sigma^2(f) = I(f^2) - I(f)^2$, then by Central Limit Theorem:

$$\lim_{N \rightarrow \infty} \mathbb{P} \left(|I(f) - I_{MC}(f)| \leq c \frac{\sigma(f)}{\sqrt{N}} \right) = \frac{1}{\sqrt{2\pi}} \int_{-c}^c e^{-x^2/2} dx. \quad (46)$$

Hence, instead of a deterministic error bound, we obtain a ‘probabilistic’ error bound with a convergence rate $\mathcal{O}(N^{-1/2})$ \square

C PROOF OF THE CONVERGENCE RATE OF QUASI MONTE CARLO METHOD

Here we give a brief proof of 1D quasi Monte Carlo method.

Proof. Consider a function $f : [0, 1] \rightarrow \mathbb{R}$ that holds:

$$f(x) = f(1) - \int_0^1 f'(y) \mathbb{1}_{[0,y]}(x) dy, \quad (47)$$

where

$$\mathbb{1}_{[0,y]}(x) = \begin{cases} 1 & \text{if } x \in [0, y], \\ 0 & \text{if } x \notin [0, y]. \end{cases} \quad (48)$$

The quasi Monte Carlo method also approximates the quadrature by a summation of a sequence set $\{x_i\}_{i=1}^N$, i.e.:

$$\int_0^1 f(x) dx \approx I_{\text{QMC}}(f) := \frac{1}{N} \sum_{i=1}^N f(x_i). \quad (49)$$

Consequently, the error of this approximation is:

$$\begin{aligned} E_{\text{QMC}} &= \left| \int_0^1 f(x) dx - \frac{1}{N} \sum_{i=1}^N f(x_i) \right|, \\ &= \left| \int_0^1 \left(- \int_0^1 \mathbb{1}_{[0,y]}(x) dx + \frac{1}{N} \sum_{i=1}^N \mathbb{1}_{[0,y]}(x_i) \right) f'(y) dy \right| \\ &= \left| \int_0^1 \Delta_P(y) f'(y) dy \right| \\ &\leq \left(\int_0^1 |\Delta_P(y)|^p dy \right)^{1/p} \left(\int_0^1 |f'(y)|^q dy \right)^{1/q} \\ &= \|\Delta_P\|_{L_q} \|f'\|_{L_q}. \end{aligned} \quad (50)$$

where $\Delta_P(y)$ is the local discrepancy of the set $P = \{x_i\}_{i=1}^N$, and

$$\Delta_P(y) := \frac{1}{N} \sum_{i=1}^N \mathbb{1}_{[0,y]}(x_i) - \int_0^1 \mathbb{1}_{[0,y]}(x) dx. \quad (51)$$

The last inequality of Eq. (50) held by Hölder's inequality, so p, q satisfy $\frac{1}{p} + \frac{1}{q} = 1$. \square

Both the term $\|f'\|_{L_q}$ and the $\sigma(f)$ in Eq. (46) are dependent on the function f , or more specifically, on the variation of f . While the $\|\Delta_P\|_{L_q}$ depends on the specific sequence used in QMC.

Additionally, if $p = \infty, q = 1$, we have

$$E_{\text{QMC}} \leq V(f) D_N^*(x_1, \dots, x_N), \quad (52)$$

where $V(f)$ is the bounded variation of f in $[0, 1]$.

D PROOF OF THEOREM 1

Suppose that $f(x) \in \mathcal{H}$ is a smooth function defined on the domain Ω , L is a smooth operator, $J(f) = \int_{\Omega} L[f] dx$, $J_N(f) = \frac{1}{N} \sum_{i=1}^N L[f(x_i)]$ where x_i is sampled on Ω . Also, suppose

$$\begin{aligned} f_N^* &= \arg \min_f J_N(f), \\ f^* &= \arg \min_f J(f). \end{aligned} \quad (53)$$

Assume that

1. f^* is the unique global minimizer.
2. The functional $J(f)$ is strongly convex with a constant $\mu > 0$ if $f \in B_r(f^*)$ and $f_N^* \in B_r(f^*)$.

we want to show $\|f_N^* - f^*\| = \mathcal{O}(\|J[f] - J_N(f)\|)$.

Proof. As $J(f)$ is strongly convex,

$$J(f) \geq J(f^*) + \langle \delta J(f^*), f - f^* \rangle + \frac{\mu}{2} \|f - f^*\|^2, \forall f \in B_r(f^*). \quad (54)$$

Since f^* is the unique global minimizer, then $\delta J(f^*) = 0$,

$$J(f) \geq J(f^*) + \frac{\mu}{2} \|f - f^*\|^2. \quad (55)$$

Let $f = f_N^*$, we can derive that

$$\frac{\mu}{2} \|f_N^* - f^*\|^2 \leq J(f_N^*) - J(f^*). \quad (56)$$

Since $J_N(f_N^*) \leq J_N(f^*)$,

$$\begin{aligned} J(f_N^*) - J(f^*) &= J(f_N^*) - J_N(f_N^*) + J_N(f_N^*) - J_N(f^*) + J_N(f^*) - J(f^*) \\ &\leq J(f_N^*) - J_N(f_N^*) + J_N(f^*) - J(f^*) \\ &\leq \|J(f_N^*) - J_N(f_N^*)\| + \|J_N(f^*) - J(f^*)\|. \end{aligned} \quad (57)$$

Herein,

$$\frac{\mu}{2} \|f_N^* - f^*\|^2 \leq \|J(f_N^*) - J_N(f_N^*)\| + \|J_N(f^*) - J(f^*)\|. \quad (58)$$

Since the scale of convergence rate $\mathcal{O}(\|J[f] - J_N(f)\|)$ is invariant for f including f^* and f_N^* . Thus

$$\|f_N^* - f^*\|^2 = \mathcal{O}(\|J[f] - J_N(f)\|) + \mathcal{O}(\|J[f] - J_N(f)\|) = \mathcal{O}(\|J[f] - J_N(f)\|). \quad (59)$$

Then, if those assumptions are satisfied for PINNs, the proof is finished. Obviously, J is the $\mathcal{L}_{int}(f)$ in Eq. (7) and J_N is the $\mathcal{L}(f)$ in Eq. (3).

For assumption 1. Since the PDE system is well defined, then the solution u is unique and $J(u) = 0$ which is the minimal value. Consequently, if $f(x)$ is smooth, then we can claim that $f^*(x) = u(x)$ for $\forall x \in \Omega$. Fortunately, in PINNs, the function f is the output of the networks, herein, the assumption of smoothness is reasonable especially the vanilla PINNs Raissi et al. (2019) embedded by tanh activation function. Herein, as u is unique, f^* is unique.

For assumption 2. Since \mathcal{N} and \mathcal{B} are differential operators, $J(f)$ is a smooth functional with respected to f . Since the solution u is unique, then $J(f) > 0$ if $f \neq u$. Combining with that $J(f)$ is smooth functional, there exist a constant r such that for any f in the compact ball $B_r(u) = \{f | \|f - u\| \leq r\}$, $\delta^2 J(f) > 0$. Furthermore, since $\delta^2 J[f]$ is bounded for $f \in B_r(u)$, then there exist a constant number $\mu > 0$ such that $\delta^2 J(f) \geq \mu, \forall f \in B_r(u)$. Consequently, $J(f)$ is strongly convex for $f \in B_r(u) = B_r(f^*)$. \square

Remark. Although in the above proof, the radius r looks like a small number. In practice, if \mathcal{N} is linear, then for any $f \in \mathcal{H}$, $J(f)$ is strongly convex (i.e. $r = \infty$); if \mathcal{N} is nonlinear, then $J(f)$ is still strongly convex for any $f \in \mathcal{H}$ if $\int \delta N^2 + \mathcal{N} \cdot \delta^2 \mathcal{N} dx \geq 0$.

E ADAPTIVE SAMPLING METHODS

E.1 RAD

Suppose $p(x)$ is the probability density function (PDF) for sampling points. Then residual-based adaptive distribution method (RAD) defines the PDF as

$$p(\mathbf{x}) \propto \frac{\varepsilon_r^k(\theta, \mathbf{x})}{\mathbb{E}[\varepsilon_r^k(\theta, \mathbf{x})]} + c, \quad (60)$$

where $k > 0$, $c > 0$ are two hyperparameters. The whole algorithm is demonstrated in Algorithm 3. In our experiments, we inherit the hyperparameters from the original RAD methods: $k = 1$, $c=1$. The size of the sampling pool is $50 \times N_r$.

Input: Number of epochs s .

Output: the output of PINN u

Generate \mathcal{P} by uniformly sampling from the domain.

Train the PINN for a certain number of iterations;

for $i = 2, \dots, s$ **do**

 Generate \mathcal{P} by randomly sampling based on the probability distribution function Eq. (60);

 Train the PINN for a certain number of iterations;

end

return the output of PINN.

Algorithm 3: RAD

E.2 ACLE

ACLE is the first algorithm to jointly optimize the selection of all training point types ($\mathbf{x}_{ic}, \mathbf{x}_{bc}, \mathbf{x}_r$ and experimental points) by automatically adjusting the proportion of collocation point types during training by leveraging the neural tangent kernel (NTK) Wang et al. (2022). Notably, in our experiments, we focus on forward problems and don't have experimental points.

Suppose $P = \{\mathbf{x}_i\}_{i=1}^N$ is the set of input points, then the $\Theta_t(P) = \{\theta_{ij}\}$ is the NTK matrix, its element $\theta_{ij} = \theta_t(\mathbf{x}_i, \mathbf{x}_j)$ computed as follows:

$$\theta_t(\mathbf{x}_i, \mathbf{x}_j) = \nabla_{\theta} \varepsilon_r(\theta, \mathbf{x}_i) (\nabla_{\theta} \varepsilon_r(\theta, \mathbf{x}_j))^{\top}. \quad (61)$$

In addition, we define $\Theta_t(\mathbf{x}, P) = \{\theta_t(\mathbf{x}, \mathbf{x}_i)\}_{i=1}^N$. And the convergence degree is defined:

$$\alpha(\mathbf{x}; t) = \sum_{i=1}^{\infty} \lambda_{t,i}^{-1} \langle \varepsilon_r(\theta_{t+1}, \mathbf{x}) - \varepsilon_r(\theta_t, \mathbf{x}), \psi_{t,i} \rangle_{\mathcal{H}_{\theta_t}}^2, \quad (62)$$

where λ_t and ψ_t are the corresponding eigenvalue and eigenvector of Θ_t , \mathcal{H}_{θ_t} is the reproducing kernel Hilbert space with the kernel Θ_t . The whole algorithm is shown in Algorithm 4. However, since the computation of Eqs. (61) and (62) is pretty complex, ACLE introduces Nystrom approximation Williams & Seeger (2000) to estimate the NTK matrix Θ_t and the convergence degree α . Although this approximation is efficient, ACLE still requires unaffordable requirements of computation when solving PDEs with $d = 100$ in our experiments.

Input: Number of epochs s .

Output: the output of PINN u

for $i = 1, \dots, s$ **do**

 Randomly sample candidate points $\mathcal{P}_{\text{pool}}$ from the domain.;

 Compute Θ_t by Eq. (61);

 Select subset $\mathcal{P} \subset \mathcal{P}_{\text{pool}}$ based on the PDF $\alpha(\mathbf{x}; t)$ computed by Eq. (62);

 Train the PINN for a certain number of iterations;

end

return the output of PINN.

Algorithm 4: ACLE

F THE ERRORS OF EXPERIMENTS

Here we provide the details of the relative error for Allen-Cahn equations and Sine-Gordon equations in appendix 3.1.

F.1 ALLEN-CAHN

For $d = 3$, with different width and depth, the results are shown in Table 4. For the vanilla model, the best result is $2.15 \times 10^{-4} \pm 3.78 \times 10^{-5}$ achieved with depth=10 and width=50. The RAD model yields the smallest mean at $3.85 \times 10^{-4} \pm 1.96 \times 10^{-4}$ with depth=10 and width=50. For the ACLE model, the optimal outcome is $5.40 \times 10^{-4} \pm 8.41 \times 10^{-5}$ with depth=10 and width=100.

The Halton model's best performance is $2.54 \times 10^{-4} \pm 3.72 \times 10^{-5}$ with depth=10 and width=50. Lastly, the Sobol model achieves the best result of $2.64 \times 10^{-4} \pm 2.11 \times 10^{-4}$ with depth=7 and width=50.

For $d = 10$, with different width and depth, the results are shown in Table 5. For the vanilla model, the best result is $2.07 \times 10^{-3} \pm 3.40 \times 10^{-5}$ achieved with depth=10 and width=70. For the RAD model, the optimal outcome is $2.12 \times 10^{-3} \pm 2.89 \times 10^{-4}$ with depth=7 and width=100. The ACLE model's best performance is $2.09 \times 10^{-3} \pm 2.19 \times 10^{-4}$ obtained with depth=7 and width=100. The Halton yields the smallest error at $2.14 \times 10^{-3} \pm 8.73 \times 10^{-5}$ with depth=7 and width=100. Lastly, the Sobol model's best result is $2.20 \times 10^{-3} \pm 6.18 \times 10^{-5}$ with depth=7 and width=70.

For $d = 100$, with different input points, the results are shown in Table 6. The results show that the best relative error achieved by Halton for Points = 1000, 2000, by Sobol for Points = 4000, 8000.

Table 4: Relative error in Allen-Cahn $d = 3$

	depth	width		
		50	70	100
vanilla	4	$3.85\text{e-}04 \pm 1.54\text{e-}04$	$7.49\text{e-}04 \pm 3.69\text{e-}04$	$4.93\text{e-}04 \pm 9.81\text{e-}05$
	5	$3.64\text{e-}04 \pm 2.60\text{e-}04$	$5.21\text{e-}04 \pm 1.27\text{e-}04$	$5.28\text{e-}04 \pm 2.31\text{e-}04$
	7	$2.26\text{e-}04 \pm 1.74\text{e-}04$	$3.37\text{e-}04 \pm 5.99\text{e-}05$	$4.94\text{e-}04 \pm 4.10\text{e-}05$
	10	$2.15\text{e-}04 \pm 3.78\text{e-}05$	$6.14\text{e-}04 \pm 7.74\text{e-}05$	$6.85\text{e-}04 \pm 1.45\text{e-}04$
RAD	4	$5.54\text{e-}04 \pm 2.80\text{e-}04$	$5.54\text{e-}04 \pm 1.18\text{e-}04$	$6.49\text{e-}04 \pm 2.37\text{e-}04$
	5	$5.42\text{e-}04 \pm 4.46\text{e-}04$	$5.01\text{e-}04 \pm 9.64\text{e-}05$	$5.92\text{e-}04 \pm 1.98\text{e-}04$
	7	$4.51\text{e-}04 \pm 2.50\text{e-}04$	$7.03\text{e-}04 \pm 1.99\text{e-}04$	$5.69\text{e-}04 \pm 1.04\text{e-}04$
	10	$3.85\text{e-}04 \pm 1.96\text{e-}04$	$7.52\text{e-}04 \pm 2.79\text{e-}04$	$4.94\text{e-}04 \pm 4.10\text{e-}05$
ACLE	4	$4.91\text{e-}04 \pm 1.56\text{e-}04$	$1.05\text{e-}03 \pm 1.79\text{e-}04$	$6.99\text{e-}04 \pm 1.74\text{e-}04$
	5	$7.90\text{e-}04 \pm 5.16\text{e-}04$	$8.42\text{e-}04 \pm 2.13\text{e-}04$	$6.24\text{e-}04 \pm 1.53\text{e-}04$
	7	$5.05\text{e-}04 \pm 1.58\text{e-}04$	$1.90\text{e-}03 \pm 1.39\text{e-}03$	$1.39\text{e-}03 \pm 5.43\text{e-}04$
	10	$5.23\text{e-}03 \pm 6.98\text{e-}03$	$2.05\text{e-}02 \pm 1.41\text{e-}02$	$5.40\text{e-}04 \pm 8.41\text{e-}05$
Helton	4	$3.99\text{e-}04 \pm 2.03\text{e-}04$	$8.34\text{e-}04 \pm 3.67\text{e-}04$	$4.77\text{e-}04 \pm 2.07\text{e-}04$
	5	$2.69\text{e-}04 \pm 1.25\text{e-}04$	$5.09\text{e-}04 \pm 1.94\text{e-}04$	$3.67\text{e-}04 \pm 1.47\text{e-}04$
	7	$3.75\text{e-}04 \pm 3.69\text{e-}04$	$3.91\text{e-}04 \pm 1.43\text{e-}04$	$4.95\text{e-}04 \pm 1.30\text{e-}04$
	10	$2.54\text{e-}04 \pm 3.72\text{e-}05$	$7.52\text{e-}04 \pm 2.79\text{e-}04$	$5.40\text{e-}04 \pm 8.41\text{e-}05$
Sobol	4	$3.89\text{e-}04 \pm 1.89\text{e-}04$	$6.17\text{e-}04 \pm 2.41\text{e-}04$	$5.18\text{e-}04 \pm 5.60\text{e-}05$
	5	$2.93\text{e-}04 \pm 1.47\text{e-}04$	$4.83\text{e-}04 \pm 1.22\text{e-}04$	$3.99\text{e-}04 \pm 1.77\text{e-}04$
	7	$2.64\text{e-}04 \pm 2.11\text{e-}04$	$4.08\text{e-}04 \pm 1.07\text{e-}04$	$5.11\text{e-}04 \pm 2.02\text{e-}04$
	10	$3.88\text{e-}04 \pm 5.65\text{e-}05$	$5.95\text{e-}04 \pm 2.21\text{e-}04$	$6.98\text{e-}04 \pm 1.01\text{e-}04$

F.2 SINE-GORDON

For $d = 3$, with different width and depth, the results are shown in Table 7. For the vanilla model, the best result is $1.26 \times 10^{-4} \pm 2.39 \times 10^{-5}$ achieved with depth=5 and width=50. The RAD model yields the smallest mean at $1.67 \times 10^{-4} \pm 3.94 \times 10^{-5}$ with depth=5 and width=50. For the ACLE model, the optimal outcome is $2.82 \times 10^{-4} \pm 2.57 \times 10^{-5}$ with depth=5 and width=50. The Halton model's best performance is $1.34 \times 10^{-4} \pm 5.43 \times 10^{-5}$ obtained with depth=7 and width=50. Lastly, the Sobol model achieves the best result of $1.14 \times 10^{-4} \pm 6.48 \times 10^{-6}$ with depth=7 and width=50.

For $d = 10$, with different width and depth, the results are shown in Table 8. For the vanilla model, the best result is $2.09 \times 10^{-3} \pm 4.08 \times 10^{-5}$ achieved with depth=7 and width=100. The RAD model yields the smallest mean at $2.43 \times 10^{-3} \pm 2.71 \times 10^{-4}$ with depth=10 and width=70. For the ACLE model, the optimal outcome is $2.41 \times 10^{-3} \pm 1.77 \times 10^{-4}$ with depth=7 and width=70. The Halton model's best performance is $2.20 \times 10^{-3} \pm 1.11 \times 10^{-4}$ obtained with depth=7 and width=100. Lastly, the Sobol model achieves the best result of $2.22 \times 10^{-3} \pm 2.05 \times 10^{-4}$ with depth=5 and width=100.

Table 5: Relative error in Allen-Cahn $d = 10$

	depth	width		
		50	70	100
vanilla	4	4.49e-03 \pm 2.87e-05	3.42e-03 \pm 1.35e-04	2.91e-03 \pm 1.38e-04
	5	3.49e-03 \pm 1.17e-04	2.69e-03 \pm 6.13e-05	2.39e-03 \pm 7.41e-05
	7	2.89e-03 \pm 9.43e-06	2.24e-03 \pm 9.09e-05	2.10e-03 \pm 1.17e-04
	10	2.62e-03 \pm 7.07e-05	2.07e-03 \pm 3.40e-05	2.08e-03 \pm 1.40e-04
RAD	4	4.62e-03 \pm 1.45e-04	3.41e-03 \pm 1.87e-04	2.98e-03 \pm 2.36e-05
	5	3.49e-03 \pm 5.73e-05	2.79e-03 \pm 1.37e-04	2.44e-03 \pm 6.16e-05
	7	2.89e-03 \pm 4.50e-05	2.33e-03 \pm 6.85e-05	2.12e-03 \pm 2.89e-04
	10	2.57e-03 \pm 1.43e-04	2.26e-03 \pm 2.08e-04	2.60e-03 \pm 2.58e-04
ACLE	4	4.79e-03 \pm 8.06e-05	3.55e-03 \pm 7.93e-05	3.12e-03 \pm 2.52e-04
	5	3.53e-03 \pm 1.44e-04	2.84e-03 \pm 1.89e-05	2.35e-03 \pm 1.48e-04
	7	2.90e-03 \pm 1.19e-04	2.33e-03 \pm 1.74e-04	2.09e-03 \pm 2.19e-04
	10	2.63e-03 \pm 2.22e-04	2.22e-03 \pm 4.90e-05	2.76e-03 \pm 3.52e-04
Halton	4	4.43e-03 \pm 4.32e-05	3.39e-03 \pm 1.23e-04	2.90e-03 \pm 1.80e-04
	5	3.57e-03 \pm 1.02e-04	2.64e-03 \pm 9.43e-06	2.37e-03 \pm 8.96e-05
	7	2.76e-03 \pm 4.92e-05	2.22e-03 \pm 5.72e-05	2.14e-03 \pm 8.73e-05
	10	2.60e-03 \pm 1.73e-04	2.24e-03 \pm 2.83e-05	2.55e-03 \pm 9.98e-05
Sobol	4	4.54e-03 \pm 1.93e-04	3.39e-03 \pm 1.23e-04	2.90e-03 \pm 1.80e-04
	5	3.57e-03 \pm 1.02e-04	2.64e-03 \pm 9.43e-06	2.29e-03 \pm 2.94e-05
	7	2.78e-03 \pm 1.10e-04	2.20e-03 \pm 6.18e-05	2.43e-03 \pm 1.89e-04
	10	2.63e-03 \pm 1.60e-04	2.24e-03 \pm 2.83e-05	2.32e-03 \pm 1.41e-04

Table 6: Relative error in Allen-Cahn $d = 100$

Points	Vanilla	RAD	Halton	Sobol
1000	1.69e-02 \pm 5.77e-05	1.69e-02 \pm 4.04e-04	1.30e-02 \pm 5.51e-04	1.71e-02 \pm 1.53e-04
2000	1.68e-02 \pm 5.77e-05	1.68e-02 \pm 3.79e-04	1.53e-02 \pm 1.57e-03	1.67e-02 \pm 5.77e-05
4000	1.70e-02 \pm 4.04e-04	1.68e-02 \pm 4.04e-04	1.70e-02 \pm 2.31e-04	1.68e-02 \pm 1.15e-04
8000	1.70e-02 \pm 1.53e-04	1.69e-02 \pm 2.89e-04	1.70e-02 \pm 8.66e-05	1.68e-02 \pm 1.15e-04

For $d = 100$, with different input points, the results are shown in Table 9. The results show that the best relative error achieved by Halton for Points = 1000, 2000, 8000. by RAD for Points = 4000.

Table 7: Relative error in Sine-Gordon $d = 3$

model	depth	width		
		50	70	100
vanilla	4	$1.76\text{e-}04 \pm 7.52\text{e-}05$	$3.07\text{e-}04 \pm 1.18\text{e-}04$	$3.25\text{e-}04 \pm 1.82\text{e-}04$
	5	$1.26\text{e-}04 \pm 2.39\text{e-}05$	$2.83\text{e-}04 \pm 7.39\text{e-}05$	$2.96\text{e-}04 \pm 1.20\text{e-}04$
	7	$2.70\text{e-}04 \pm 1.53\text{e-}04$	$4.16\text{e-}04 \pm 1.41\text{e-}04$	$1.01\text{e-}03 \pm 5.99\text{e-}04$
	10	$5.07\text{e-}04 \pm 3.98\text{e-}04$	$8.49\text{e-}04 \pm 1.40\text{e-}04$	$6.37\text{e-}04 \pm 2.55\text{e-}04$
RAD	4	$2.24\text{e-}04 \pm 9.63\text{e-}05$	$4.04\text{e-}04 \pm 1.55\text{e-}04$	$4.03\text{e-}04 \pm 1.96\text{e-}04$
	5	$1.67\text{e-}04 \pm 3.94\text{e-}05$	$3.67\text{e-}04 \pm 1.41\text{e-}04$	$4.70\text{e-}04 \pm 2.34\text{e-}04$
	7	$2.77\text{e-}04 \pm 1.57\text{e-}04$	$4.16\text{e-}04 \pm 1.41\text{e-}04$	$1.01\text{e-}03 \pm 5.99\text{e-}04$
	10	$2.48\text{e-}04 \pm 1.09\text{e-}04$	$8.27\text{e-}04 \pm 5.62\text{e-}05$	$9.06\text{e-}04 \pm 5.59\text{e-}04$
ACLE	4	$3.46\text{e-}04 \pm 7.83\text{e-}05$	$2.86\text{e-}04 \pm 8.38\text{e-}05$	$4.87\text{e-}04 \pm 1.70\text{e-}04$
	5	$2.82\text{e-}04 \pm 2.57\text{e-}05$	$4.03\text{e-}04 \pm 1.69\text{e-}04$	$4.47\text{e-}04 \pm 8.44\text{e-}05$
	7	$3.35\text{e-}04 \pm 2.22\text{e-}05$	$1.32\text{e-}03 \pm 1.29\text{e-}03$	$2.04\text{e-}03 \pm 6.17\text{e-}04$
	10	$4.55\text{e-}04 \pm 2.12\text{e-}04$	$8.77\text{e-}04 \pm 1.86\text{e-}04$	$1.02\text{e-}03 \pm 3.43\text{e-}04$
Halton	4	$2.32\text{e-}04 \pm 1.07\text{e-}04$	$2.61\text{e-}04 \pm 7.45\text{e-}05$	$2.87\text{e-}04 \pm 1.47\text{e-}04$
	5	$1.73\text{e-}04 \pm 4.52\text{e-}05$	$3.06\text{e-}04 \pm 1.34\text{e-}04$	$3.61\text{e-}04 \pm 1.26\text{e-}04$
	7	$1.34\text{e-}04 \pm 5.43\text{e-}05$	$3.31\text{e-}04 \pm 8.20\text{e-}05$	$8.93\text{e-}04 \pm 3.70\text{e-}04$
	10	$2.48\text{e-}04 \pm 1.09\text{e-}04$	$8.27\text{e-}04 \pm 5.62\text{e-}05$	$1.01\text{e-}03 \pm 5.99\text{e-}04$
Sobol	4	$1.57\text{e-}04 \pm 4.09\text{e-}05$	$3.29\text{e-}04 \pm 1.51\text{e-}04$	$2.75\text{e-}04 \pm 6.22\text{e-}05$
	5	$1.58\text{e-}04 \pm 4.12\text{e-}05$	$3.93\text{e-}04 \pm 9.10\text{e-}05$	$3.06\text{e-}04 \pm 1.33\text{e-}04$
	7	$1.14\text{e-}04 \pm 6.48\text{e-}06$	$7.40\text{e-}04 \pm 3.53\text{e-}04$	$7.92\text{e-}04 \pm 3.59\text{e-}04$
	10	$3.17\text{e-}04 \pm 2.82\text{e-}04$	$9.69\text{e-}04 \pm 6.32\text{e-}04$	$7.76\text{e-}04 \pm 3.31\text{e-}04$

G DETAILS OF COST

For the experiments of generating the low-discrepancy sequences, we warm-up 2 times and run 20 times to obtain the expectation and the standard deviation. The used package is SciPy Virtanen et al. (2020). Fig. 9 has already indicated that both the memory consumption and the execution time exhibit a linear dependence on N . However, based on the detail shown in Tables 10 to 13, the memory consumption is also linear dependent on d while the execution time is not. Furthermore, because of the difference of the generating algorithm, Halton sequences and Sobol' sequences exhibit different sensitivities to dimensionality, with Sobol showing a more pronounced increase than Halton in computation time under high-dimensional problems.

H ABLATION STUDY

Except the $d = 100$ experiments in Table 2, we also conducted the experiments of Poisson's equations Eq. (25) for $d = 3$ and $d = 100$ and the results are shown in Table 14. The results reveals that, replacing the sampling pool by low-discrepancy sequences is more accurate for RAD, the corresponding maximum promotion is 69.4% when $\alpha = 10$ and $d = 3$. However, when implementing ACLE methods, low-discrepancy sequences are invalid and decrease the accuracy. We argue that randomly sampling the P_{pool} is better to detect the convergence degree α . Herein, utilizing low-discrepancy sequences will reduce the infinite P_{pool} to a finite point set, although it can be alleviated by increasing N_{scale} .

Table 8: Relative error in Sine-Gordon $d = 10$

	depth	width		
		50	70	100
vanilla	4	5.34e-03 \pm 3.17e-04	4.11e-03 \pm 1.17e-04	3.09e-03 \pm 1.72e-04
	5	4.23e-03 \pm 1.79e-04	2.97e-03 \pm 2.17e-04	2.41e-03 \pm 8.83e-05
	7	3.01e-03 \pm 1.20e-04	2.56e-03 \pm 1.40e-04	2.09e-03 \pm 4.08e-05
	10	2.86e-03 \pm 2.38e-04	2.18e-03 \pm 1.16e-04	3.10e-03 \pm 2.33e-04
RAD	4	5.61e-03 \pm 5.59e-04	3.93e-03 \pm 3.00e-04	3.19e-03 \pm 3.67e-04
	5	4.52e-03 \pm 3.23e-04	3.03e-03 \pm 1.06e-04	2.63e-03 \pm 2.12e-04
	7	3.49e-03 \pm 5.70e-04	2.81e-03 \pm 2.01e-04	3.10e-03 \pm 9.47e-04
	10	2.70e-03 \pm 1.57e-04	2.43e-03 \pm 2.71e-04	3.89e-03 \pm 5.81e-04
ACLE	4	5.51e-03 \pm 4.54e-04	4.09e-03 \pm 1.45e-04	3.36e-03 \pm 2.35e-04
	5	4.35e-03 \pm 4.99e-04	3.15e-03 \pm 3.77e-05	2.53e-03 \pm 2.12e-04
	7	3.28e-03 \pm 1.58e-04	2.41e-03 \pm 1.77e-04	2.64e-03 \pm 4.20e-04
	10	3.13e-03 \pm 3.06e-04	2.74e-03 \pm 5.31e-04	2.84e-03 \pm 3.50e-04
Halton	4	5.49e-03 \pm 1.79e-04	4.02e-03 \pm 7.32e-05	3.21e-03 \pm 1.45e-04
	5	4.55e-03 \pm 2.67e-04	2.99e-03 \pm 2.26e-04	2.72e-03 \pm 4.64e-05
	7	3.07e-03 \pm 6.94e-05	2.48e-03 \pm 2.13e-04	2.20e-03 \pm 1.11e-04
	10	2.86e-03 \pm 1.74e-04	2.49e-03 \pm 3.35e-04	3.08e-03 \pm 4.42e-04
Sobol	4	5.40e-03 \pm 2.24e-04	4.00e-03 \pm 6.60e-05	3.01e-03 \pm 1.05e-04
	5	4.27e-03 \pm 9.80e-05	2.93e-03 \pm 8.16e-05	2.55e-03 \pm 4.92e-05
	7	3.17e-03 \pm 1.21e-04	2.59e-03 \pm 1.03e-04	2.53e-03 \pm 2.28e-04
	10	2.82e-03 \pm 1.07e-04	2.22e-03 \pm 2.05e-04	3.16e-03 \pm 3.69e-04

Table 9: Relative error in Sine-Gordon $d = 100$

Points	Vanilla	RAD	Halton	Sobol
1000	1.09e-02 \pm 2.00e-04	1.09e-02 \pm 3.51e-04	7.33e-03 \pm 1.49e-04	1.08e-02 \pm 3.06e-04
2000	1.09e-02 \pm 3.61e-04	1.08e-02 \pm 2.65e-04	7.90e-03 \pm 1.15e-04	1.10e-02 \pm 2.65e-04
4000	1.10e-02 \pm 2.52e-04	1.09e-02 \pm 1.53e-04	1.09e-02 \pm 3.06e-04	1.09e-02 \pm 2.52e-04
8000	1.10e-02 \pm 1.53e-04	1.09e-02 \pm 2.52e-04	1.08e-02 \pm 3.06e-04	1.10e-02 \pm 5.77e-05

Table 10: Halton Execution Time (ms)

N	dim		
	3	10	50
100	$3.20 \times 10^{-1} \pm 2.02 \times 10^{-2}$	$2.81 \times 10^{-1} \pm 1.27 \times 10^{-2}$	$4.49 \times 10^{-1} \pm 9.88 \times 10^{-3}$
2000	$4.71 \times 10^{-1} \pm 1.24 \times 10^{-2}$	$5.56 \times 10^{-1} \pm 1.37 \times 10^{-2}$	$1.28 \times 10^0 \pm 3.13 \times 10^{-2}$
4000	$6.70 \times 10^{-1} \pm 1.04 \times 10^{-2}$	$2.92 \times 10^0 \pm 8.86 \times 10^0$	$2.16 \times 10^0 \pm 3.33 \times 10^{-2}$
8000	$1.20 \times 10^0 \pm 2.92 \times 10^{-1}$	$1.57 \times 10^0 \pm 7.20 \times 10^{-2}$	$4.00 \times 10^0 \pm 2.85 \times 10^{-2}$
16000	$2.08 \times 10^0 \pm 4.41 \times 10^{-2}$	$2.98 \times 10^0 \pm 1.01 \times 10^{-1}$	$7.96 \times 10^0 \pm 9.03 \times 10^{-2}$
32000	$4.16 \times 10^0 \pm 9.41 \times 10^{-2}$	$6.10 \times 10^0 \pm 1.92 \times 10^{-1}$	$1.74 \times 10^1 \pm 1.09 \times 10^0$
64000	$6.76 \times 10^0 \pm 2.25 \times 10^{-1}$	$1.27 \times 10^1 \pm 2.98 \times 10^{-1}$	$3.73 \times 10^1 \pm 8.06 \times 10^{-1}$
128000	$1.42 \times 10^1 \pm 4.88 \times 10^{-1}$	$2.67 \times 10^1 \pm 4.59 \times 10^{-1}$	$8.59 \times 10^1 \pm 2.56 \times 10^{-1}$
256000	$3.03 \times 10^1 \pm 9.14 \times 10^{-1}$	$5.67 \times 10^1 \pm 1.16 \times 10^0$	$2.05 \times 10^2 \pm 2.78 \times 10^0$
512000	$6.76 \times 10^1 \pm 6.25 \times 10^0$	$1.29 \times 10^2 \pm 2.97 \times 10^{-1}$	$4.46 \times 10^2 \pm 3.07 \times 10^0$
1024000	$1.47 \times 10^2 \pm 1.84 \times 10^1$	$2.97 \times 10^2 \pm 2.16 \times 10^0$	$9.53 \times 10^2 \pm 1.93 \times 10^0$

Table 11: Sobol Execution Time (ms)

N	dim		
	3	10	50
100	$3.46 \times 10^{-1} \pm 5.40 \times 10^{-2}$	$2.68 \times 10^{-1} \pm 8.64 \times 10^{-3}$	$2.82 \times 10^{-1} \pm 8.24 \times 10^{-3}$
2000	$3.53 \times 10^{-1} \pm 1.48 \times 10^{-2}$	$3.09 \times 10^{-1} \pm 1.50 \times 10^{-2}$	$4.25 \times 10^{-1} \pm 1.14 \times 10^{-2}$
4000	$3.79 \times 10^{-1} \pm 1.04 \times 10^{-2}$	$3.57 \times 10^{-1} \pm 1.55 \times 10^{-2}$	$5.51 \times 10^{-1} \pm 1.79 \times 10^{-2}$
8000	$4.43 \times 10^{-1} \pm 1.62 \times 10^{-2}$	$4.31 \times 10^{-1} \pm 1.90 \times 10^{-2}$	$7.85 \times 10^{-1} \pm 2.14 \times 10^{-2}$
16000	$5.55 \times 10^{-1} \pm 2.63 \times 10^{-2}$	$5.96 \times 10^{-1} \pm 6.10 \times 10^{-2}$	$1.24 \times 10^0 \pm 1.99 \times 10^{-2}$
32000	$8.61 \times 10^{-1} \pm 4.56 \times 10^{-1}$	$8.89 \times 10^{-1} \pm 1.00 \times 10^{-1}$	$2.38 \times 10^0 \pm 1.70 \times 10^{-1}$
64000	$7.61 \times 10^{-1} \pm 1.08 \times 10^{-1}$	$1.46 \times 10^0 \pm 1.44 \times 10^{-1}$	$5.52 \times 10^0 \pm 2.18 \times 10^0$
128000	$2.20 \times 10^0 \pm 7.10 \times 10^{-1}$	$2.92 \times 10^0 \pm 6.64 \times 10^{-1}$	$2.75 \times 10^1 \pm 1.99 \times 10^{-1}$
256000	$3.42 \times 10^0 \pm 1.03 \times 10^0$	$5.37 \times 10^0 \pm 9.74 \times 10^{-1}$	$5.35 \times 10^1 \pm 2.19 \times 10^{-1}$
512000	$1.08 \times 10^1 \pm 3.99 \times 10^0$	$2.51 \times 10^1 \pm 1.19 \times 10^0$	$1.06 \times 10^2 \pm 1.05 \times 10^0$
1024000	$1.27 \times 10^1 \pm 4.13 \times 10^0$	$4.87 \times 10^1 \pm 2.09 \times 10^0$	$2.08 \times 10^2 \pm 5.55 \times 10^{-1}$

I DETAILS OF STOCHASTIC TAYLOR DERIVATIVE ESTIMATOR

I.1 INTRODUCTION

The Stochastic Taylor Derivative Estimator (STDE) is a novel framework designed to efficiently estimate arbitrary high-order or high-dimensional differential operators, addressing the critical computational bottlenecks of traditional automatic differentiation (AD) methods. STDE bridges the gap between univariate high-order AD (Taylor mode) and multivariate derivative tensor contractions, enabling scalable and accurate computation of high-dimensional and high-order differential operators that are intractable for conventional methods.

Given a function $u : \mathbb{R}^d \rightarrow \mathbb{R}$, a differentiable operator \mathcal{L} can be expressed by:

$$\mathcal{L}u(x) = \sum_{\alpha \in \mathcal{I}(\mathcal{L})} C_\alpha \mathcal{D}^\alpha u(x), \quad (63)$$

where $\alpha = (\alpha_1, \alpha_2, \dots, \alpha_d)$ is a multi-index, $\mathcal{D}^\alpha = \frac{\partial^{|\alpha|}}{\partial x_1^{\alpha_1} \dots \partial x_d^{\alpha_d}}$ denotes the partial derivative of order $|\alpha| = \sum \alpha_i$, and C_α are coefficients defining the operator \mathcal{L} . Eq. (63) can be rewritten using tensor contractions:

$$\mathcal{L}u(x) = D_u^k(x) \cdot C(\mathcal{L}), \quad (64)$$

Table 12: Halton Memory Usage (KB)

N	dim		
	3	10	50
100	$3.21 \times 10^0 \pm 5.23 \times 10^{-3}$	$1.02 \times 10^1 \pm 0.00 \times 10^0$	$5.11 \times 10^1 \pm 0.00 \times 10^0$
2000	$4.88 \times 10^1 \pm 0.00 \times 10^0$	$1.62 \times 10^2 \pm 0.00 \times 10^0$	$8.11 \times 10^2 \pm 0.00 \times 10^0$
4000	$9.68 \times 10^1 \pm 0.00 \times 10^0$	$3.22 \times 10^2 \pm 5.23 \times 10^{-3}$	$1.61 \times 10^3 \pm 0.00 \times 10^0$
8000	$1.93 \times 10^2 \pm 0.00 \times 10^0$	$6.42 \times 10^2 \pm 0.00 \times 10^0$	$3.21 \times 10^3 \pm 0.00 \times 10^0$
16000	$3.85 \times 10^2 \pm 0.00 \times 10^0$	$1.28 \times 10^3 \pm 0.00 \times 10^0$	$6.41 \times 10^3 \pm 0.00 \times 10^0$
32000	$7.69 \times 10^2 \pm 0.00 \times 10^0$	$2.56 \times 10^3 \pm 0.00 \times 10^0$	$1.28 \times 10^4 \pm 0.00 \times 10^0$
64000	$1.54 \times 10^3 \pm 0.00 \times 10^0$	$5.12 \times 10^3 \pm 0.00 \times 10^0$	$2.56 \times 10^4 \pm 0.00 \times 10^0$
128000	$3.07 \times 10^3 \pm 0.00 \times 10^0$	$1.02 \times 10^4 \pm 0.00 \times 10^0$	$5.12 \times 10^4 \pm 0.00 \times 10^0$
256000	$6.14 \times 10^3 \pm 0.00 \times 10^0$	$2.05 \times 10^4 \pm 0.00 \times 10^0$	$1.02 \times 10^5 \pm 0.00 \times 10^0$
512000	$1.23 \times 10^4 \pm 0.00 \times 10^0$	$4.10 \times 10^4 \pm 0.00 \times 10^0$	$2.05 \times 10^5 \pm 0.00 \times 10^0$
1024000	$2.46 \times 10^4 \pm 0.00 \times 10^0$	$8.19 \times 10^4 \pm 0.00 \times 10^0$	$4.10 \times 10^5 \pm 0.00 \times 10^0$

Table 13: Sobol Memory Usage (KB)

N	dim		
	3	10	50
100	$2.68 \times 10^0 \pm 0.00 \times 10^0$	$8.28 \times 10^0 \pm 0.00 \times 10^0$	$4.03 \times 10^1 \pm 0.00 \times 10^0$
2000	$4.83 \times 10^1 \pm 0.00 \times 10^0$	$1.60 \times 10^2 \pm 0.00 \times 10^0$	$8.00 \times 10^2 \pm 0.00 \times 10^0$
4000	$9.63 \times 10^1 \pm 0.00 \times 10^0$	$3.20 \times 10^2 \pm 0.00 \times 10^0$	$1.60 \times 10^3 \pm 0.00 \times 10^0$
8000	$1.92 \times 10^2 \pm 0.00 \times 10^0$	$6.40 \times 10^2 \pm 0.00 \times 10^0$	$3.20 \times 10^3 \pm 0.00 \times 10^0$
16000	$3.84 \times 10^2 \pm 0.00 \times 10^0$	$1.28 \times 10^3 \pm 0.00 \times 10^0$	$6.40 \times 10^3 \pm 0.00 \times 10^0$
32000	$7.68 \times 10^2 \pm 0.00 \times 10^0$	$2.56 \times 10^3 \pm 0.00 \times 10^0$	$1.28 \times 10^4 \pm 0.00 \times 10^0$
64000	$1.54 \times 10^3 \pm 0.00 \times 10^0$	$5.12 \times 10^3 \pm 0.00 \times 10^0$	$2.56 \times 10^4 \pm 0.00 \times 10^0$
128000	$3.07 \times 10^3 \pm 0.00 \times 10^0$	$1.02 \times 10^4 \pm 0.00 \times 10^0$	$5.12 \times 10^4 \pm 0.00 \times 10^0$
256000	$6.14 \times 10^3 \pm 0.00 \times 10^0$	$2.05 \times 10^4 \pm 0.00 \times 10^0$	$1.02 \times 10^5 \pm 0.00 \times 10^0$
512000	$1.23 \times 10^4 \pm 0.00 \times 10^0$	$4.10 \times 10^4 \pm 0.00 \times 10^0$	$2.05 \times 10^5 \pm 0.00 \times 10^0$
1024000	$2.46 \times 10^4 \pm 0.00 \times 10^0$	$8.19 \times 10^4 \pm 0.00 \times 10^0$	$4.10 \times 10^5 \pm 0.00 \times 10^0$

where $D_u^k(x) \in \mathbb{R}^{d^k}$ is the k -th order derivative tensor of u at x , $C(\mathcal{L}) \in \mathbb{R}^{d^k}$ is the coefficient tensor (with entries C_α at positions corresponding to α), and \cdot denotes tensor dot product.

To estimate $\mathcal{L}u(x)$, STDE constructs random jets such that the expectation of $\partial^l u(J_g^l)$ over jet samples equals the target contraction $D_u^k(x) \cdot C(\mathcal{L})$. Formally, for a distribution p over l -jets, we require:

$$\mathbb{E}_{J_g^l \sim p} [\partial^l u(J_g^l)] = D_u^k(x) \cdot C(\mathcal{L}). \quad (65)$$

This is achieved by designing p such that the expected value of the tangent product tensor matches $C(\mathcal{L})$:

$$\mathbb{E} \left[\bigotimes_{i=1}^k v^{(v_i)} \right] = C(\mathcal{L}), \quad (66)$$

where $v^{(v_i)}$ denotes the v_i -th tangent in the jet.

By averaging over multiple jet samples, STDE produces a stochastic estimator of $\mathcal{L}u(x)$ with computational complexity $O(k^2 dL)$ (where L is the number of operations in the forward graph) and memory complexity $O(kd)$, avoiding the exponential scaling in k and polynomial scaling in d of traditional methods. This efficiency enables STDE to handle differential operators of high-order and high-dimension.

Table 14: Ablation study $d = 3$ and $d = 10$

d	α	Sampling Pool	RAD	ACLE
3	1	Vanilla	$2.00e-04 \pm 9.83e-05$	$9.90e-05 \pm 3.41e-05$
		Halton	$1.77e-04 \pm 7.85e-05$	$3.06e-04 \pm 1.33e-04$
		Sobol	$6.72e-05 \pm 1.21e-05$	$2.40e-04 \pm 1.41e-04$
	10	Vanilla	$3.11e-03 \pm 1.84e-03$	$1.04e-03 \pm 3.30e-04$
		Halton	$9.49e-04 \pm 5.74e-04$	$2.30e-03 \pm 1.06e-02$
		Sobol	$1.44e-03 \pm 1.50e-04$	$4.37e-03 \pm 2.87e-03$
	100	Vanilla	$5.51e-02 \pm 1.22e-02$	$7.68e-02 \pm 2.70e-02$
		Halton	$6.12e-02 \pm 1.69e-02$	$2.29e-01 \pm 1.02e-01$
		Sobol	$6.42e-02 \pm 6.24e-03$	$2.19e-01 \pm 4.60e-02$
	1	Vanilla	$1.04e-03 \pm 3.27e-04$	$7.98e-04 \pm 4.85e-05$
		Halton	$8.18e-04 \pm 4.55e-05$	$8.22e-04 \pm 1.12e-04$
		Sobol	$8.46e-04 \pm 1.06e-04$	$8.23e-04 \pm 5.63e-05$
10	10	Vanilla	$3.31e-02 \pm 1.80e-02$	$1.89e-02 \pm 2.93e-03$
		Halton	$1.88e-02 \pm 3.02e-03$	$2.43e-02 \pm 6.94e-03$
		Sobol	$2.62e-02 \pm 2.87e-03$	$2.85e-02 \pm 1.19e-03$
	100	Vanilla	$1.86e+00 \pm 7.17e-01$	$1.04e+00 \pm 3.86e-02$
		Halton	$9.63e-01 \pm 2.52e-02$	$4.01e+00 \pm 4.66e+00$
		Sobol	$3.32e+01 \pm 5.23e+01$	$4.55e+00 \pm 2.81e+00$

I.2 EQUATIONS

In STDE, we consider the following three PDEs:

- Semi-linear Heat equation.

$$\mathcal{L}u(\mathbf{x}, t) = \nabla^2 u(\mathbf{x}, t) + \frac{1 - u(\mathbf{x}, t)^2}{1 + u(\mathbf{x}, t)^2}, \quad (\mathbf{x}, t) \in [-0.5, 0.5]^d \times [0, T]. \quad (67)$$

with initial condition $u(\mathbf{x}, 0) = 5/(10 + 2\|\mathbf{x}\|^2)$,

- Allen-Cahn equation

$$\mathcal{L}u(\mathbf{x}, t) = \nabla^2 u(\mathbf{x}, t) + u(\mathbf{x}, t) - u(\mathbf{x}, t)^3, \quad (\mathbf{x}, t) \in [-0.5, 0.5]^d \times [0, T]. \quad (68)$$

with initial condition $u(\mathbf{x}, 0) = \arctan(\max_i x_i)$,

- Sine-Gordon equation

$$\mathcal{L}u(\mathbf{x}, t) = \nabla^2 u(\mathbf{x}, t) + \sin(u(\mathbf{x}, t)), \quad (\mathbf{x}, t) \in [-0.5, 0.5]^d \times [0, T]. \quad (69)$$

with initial condition $u(\mathbf{x}, 0) = 5/(10 + 2\|\mathbf{x}\|^2)$,

All three equation uses the test point $\mathbf{x}_{\text{test}} = \mathbf{0}$ and terminal time $T = 0.3$. The used numerical solution $u(\mathbf{0}, 0.3)$ is listed in Table 15.

Table 15: Numerical solution $u(\mathbf{0}, 0.3)$

Equation	d	$u(\mathbf{0}, 0.3)$
Allen-Cahn	10^2	1.04510
	10^3	1.09100
	10^4	1.11402
Heat	10^2	0.31674
	10^3	0.28753
	10^4	0.28433
Sine-Gordon	10^2	0.0528368
	10^3	0.0055896
	10^4	0.0005621